

AD-A048 361

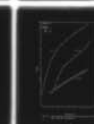
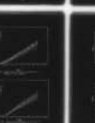
AIR FORCE INST OF TECH WRIGHT-PATTERSON AFB OHIO SCH--ETC F/G 18/8  
EFFECTS OF GAMMA RADIATION ON GALLIUM-ARSENIDE LASERS. (U)  
DEC 77 H ACKERMANN  
AFIT/GEP/PH/77-1

UNCLASSIFIED

NL

| of |

ADA048361



END  
DATE  
FILMED  
2-78  
DDC

(1)

DDC  
JAN 16 1978  
F

EFFECTS OF GAMMA RADIATION ON  
GALLIUM-ARSENIDE LASERS

Thesis

GEP/PH/77-1

Harro Ackermann  
Captain USAF

Approved for public release; distribution unlimited.

GEP/PH/77-1

EFFECTS OF GAMMA RADIATION ON  
GALLIUM-ARSENIDE LASERS

Thesis

Presented to the Faculty of the School of Engineering  
of the Air Force Institute of Technology  
Air University  
in Partial Fulfillment of the  
Requirements for the Degree of  
Master of Science

by

Harro Ackermann, B.S.

Captain USAF

Graduate Engineering Physics

December 1977

Approved for public release; distribution unlimited.

ACCESSION for	White Section	<input checked="" type="checkbox"/>
NTIS	B.H.F. Section	<input type="checkbox"/>
DDC		<input type="checkbox"/>
NAVJAG/NOJAG		
U.S. ICA 13N		
BY	DISTRIBUTION/AVAILABILITY CODES	
	SPECIAL	
A		

Preface

Captain Armen Mardiguan of the Air Force Weapons Laboratory (AFSC) proposed and sponsored this project. I extend to him my sincere appreciation for providing the injection laser samples and for supporting the project throughout its course.

My special thanks are reserved for my faculty advisors, Drs. Robert Hengehold and George John. They allowed independent work and yet provided valuable ideas and suggestions at appropriate times.

I must also express my appreciation to Sandia Laboratories for making available their gamma irradiation facility.

Harro Ackermann

Table of Contents

	<u>Page</u>
Preface . . . . .	ii
List of Figures . . . . .	iv
List of Tables . . . . .	v
Abstract . . . . .	vii
I. Introduction . . . . .	1
II. Theory . . . . .	4
General . . . . .	4
The Injection Laser . . . . .	4
Current Flow in the Injection Laser . . . . .	7
Effect of Gamma Radiation on Current . . . . .	8
Effect of Gamma Radiation on Power Output . . . . .	10
Determination of Current Flow Mechanisms . . . . .	13
Shift of Emission Peak . . . . .	13
Radiation Induced Beam Changes . . . . .	14
III. Description of Samples and Experiments . . . . .	16
IV. Results and Discussion . . . . .	21
General . . . . .	21
Pre-Irradiation Performance . . . . .	21
Measured Effect of Radiation on Threshold Current . . . . .	25
Measured Effect of Radiation on Power Output . . . . .	30
Power Output-Voltage, Current-Voltage, and Damage Factors . . . . .	32
Efficiency . . . . .	40
Emission Peak Shift . . . . .	41
Intensity Distribution and Beam Divergence . . . . .	41
V. Conclusions . . . . .	50
VI. Recommendations . . . . .	51
Bibliography . . . . .	52
Vita . . . . .	53

List of Figures

<u>Figure</u>		<u>Page</u>
1	Forward-Biased p-n Junction . . . . .	5
2	Cross-Section of Laser Package . . . . .	6
3	Front View of Typical Stripe Geometry AlGaAs Injection Laser . . . . .	6
4	Circuit for Measuring I-V, P-V Relationships . . . . .	17
5	Configuration for Obtaining Spectral Data . . . . .	19
6	Shift of Emission Peak with Applied Voltage at 77°K, Pre-Irradiation	
	a. Sample 1 . . . . .	23
	b. Sample 2 . . . . .	23
7	Shift of Emission Peak with Applied Voltage at 77°K, Pre-Irradiation	
	a. Sample 66 . . . . .	24
	b. Sample 68 . . . . .	24
8	Pre-Irradiation Power-Voltage and Current-Voltage Relation at 77°K	
	a. Samples 1 and 2 . . . . .	26
	b. Samples 66 and 68 . . . . .	26
9	Pre-Irradiation Power Efficiency at 77°K	
	a. Samples 1 and 2 . . . . .	27
	b. Samples 66 and 68 . . . . .	27
10	Power-Current Relation as Function of Dosage at 77°K	
	a. Sample 1 . . . . .	28
	b. Sample 2 . . . . .	28
	c. Sample 66 . . . . .	29
	d. Sample 68 . . . . .	29
11	Power-Voltage and Current-Voltage Relation at 77°K, Pre- and Post-Irradiation (Sample 1) . . . . .	33
12	Power-Voltage and Current-Voltage Relation at 77°K, Pre- and Post-Irradiation (Sample 2) . . . . .	34
13	Power-Voltage and Current-Voltage Relation at 77°K, Pre- and Post-Irradiation (Sample 66) . . . . .	35

List of Figures (Contd)

<u>Figure</u>		<u>Page</u>
14	Power-Voltage and Current-Voltage Relation at 77°K, Pre- and Post-Irradiation (Sample 68) . . . . .	36
15	Constant Voltage and Constant Current Change in Power Output at 77°K	
	a. Sample 1 . . . . .	38
	b. Sample 2 . . . . .	38
	c. Sample 66 . . . . .	39
	d. Sample 68 . . . . .	39
16	Power Efficiency at 77°K for Selected Dosages	
	a. Sample 1 . . . . .	42
	b. Sample 2 . . . . .	42
	c. Sample 66 . . . . .	43
	d. Sample 68 . . . . .	43
17	Intensity Distribution in Far Field, Pre- and Post-Irradiation, Sample 1	
	a. Parallel to Junction . . . . .	45
	b. Perpendicular to Junction . . . . .	45
18	Intensity Distribution in Far Field, Pre- and Post-Irradiation, Sample 2	
	a. Parallel to Junction . . . . .	46
	b. Perpendicular to Junction . . . . .	46
19	Intensity Distribution in Far Field, Pre- and Post-Irradiation, Sample 66	
	a. Parallel to Junction . . . . .	47
	b. Perpendicular to Junction . . . . .	47
20	Intensity Distribution in Far Field, Pre- and Post-Irradiation, Sample 68	
	a. Parallel to Junction . . . . .	48
	b. Perpendicular to Junction . . . . .	48

List of Tables

<u>Table</u>		<u>Page</u>
I	Typical Operating Characteristics at Room Temperature as Provided by Manufacturer . . . . .	16
II	Specific Information Provided by Manufacturer . . .	16
III	Measured Pre-Irradiation Characteristics at Room Temperature . . . . .	22
IV	Measured Pre-Irradiation Characteristics at 77°K .	22
V	Threshold Current as Function of Dosage . . . . .	30
VI	Post-Irradiation Power Output at Specific Forward Currents . . . . .	30
VII	Calculated Damage Factors, $\tau_0K$ . . . . .	37
VIII	Emission Peak Measured at Constant Current as Function of Dosage . . . . .	44
IX	Beam Divergence Before and After Irradiation . . .	44

Abstract

The effect of gamma radiation from a  $\text{Co}^{60}$  source on the performance of two types of aluminum gallium arsenide injection lasers was investigated. Both types of lasers were designed to operate in the continuous wave mode at room temperature.

Measurements were conducted to determine radiation induced changes in the threshold current, power output, efficiency, and the spectral and intensity distributions. Damage factors were calculated by the constant voltage and constant current methods.

Type C30127 (RCA) exhibited rapid degradation. A dosage of  $10^4 \text{Rad(Si)}$  reduced the output power by a factor of two. Threshold current increased, efficiency decreased, and the intensity distribution changed drastically. The damage factor at constant voltage was calculated to be  $\sim 1.5 \times 10^{-7} \text{Rad}^{-1}$ .

The performance of LCW-10 (Laser Diode Laboratories, Inc.) improved to a dosage of  $10^6 \text{Rad(Si)}$  before the onset of degradation. After  $10^8 \text{Rad(Si)}$ , power output was still comparable to pre-irradiation values. No significant changes in beam characteristics were noted. The damage factor at constant voltage was  $\sim 4 \times 10^{-8} \text{Rad}^{-1}$ .

EFFECTS OF GAMMA RADIATION ON  
GALLIUM-ARSENIDE LASERS

I. Introduction

Some proposed applications of injection lasers require their operation in a nuclear radiation environment. It is therefore necessary to obtain a knowledge of the effects of radiation on laser performance. Radiation damage studies provide this knowledge and also give some insight into the physical processes occurring in the devices. In this study the performance changes induced by gamma rays from  $\text{Co}^{60}$  were measured for two types of aluminum gallium arsenide injection lasers: Type C30127, manufactured by RCA, and type LCW-10 by Laser Diode Laboratories, Inc. Both types of lasers were designed for continuous wave operation at room temperature.

The effects of various types of radiation on gallium-arsenide compounds and on pulsed gallium-arsenide lasers have been investigated extensively by other workers. Aukerman, et al. studied the effects of fast neutrons and electrons on the gallium-arsenide crystal and determined that a decrease in carrier density and mobility occurs (Ref 1:3590-3599). With different co-workers he then investigated the effect of electron irradiation on the power output as a function of doping concentration and determined that a component of the emitted intensity remained unaffected by irradiation (Ref 2:174-180). Saji and Inuishi, working with pulsed gallium-arsenide lasers at liquid nitrogen temperature, noticed, after exposing the sample to  $\text{Co}^{60}$ , shifts in the emission peaks, as well as a decrease in efficiency and an increase in

the threshold current. They postulated that the increase in threshold current was caused by indirect recombination centers associated with the radiation induced defects (Ref 8:830-831).

Other investigators attributed the increase in threshold current to a decrease in the electro-luminescent efficiency or to an increased optical absorption in the active region (Ref 5:55-61). The decrease in output and efficiency is attributed to the introduction of non-radiative recombination centers which compete with radiative centers for the excess carriers injected. The effect of these non-radiative centers is to decrease the non-radiative lifetime and the total carrier lifetime (Ref 3:4746).

Share, et al. in later work found these explanations insufficient to account for the exponential decrease in efficiency which they observed, and introduced the concept of the luminescent killer center to explain their results (Ref 9:471-480). They suggested that defects were introduced which quenched the radiative recombination process in a volume extending over several radiative recombination centers.

In the present work the effects of gamma radiation from  $\text{Co}^{60}$  on two types of continuous-wave, room temperature aluminum-gallium-arsenide lasers were investigated. Performance was characterized by measuring current vs voltage and power output vs voltage relationships, calculating efficiency, and obtaining spectral and intensity distributions. Damage factors were calculated for both types of lasers by the constant voltage and constant current methods.

Specific gamma radiation induced effects are discussed in more detail in Section II. The individual measurements are described in

Section III, and experimental results are presented and discussed in Section IV. Section V summarizes the findings of this investigation, and suggestions for additional work are contained in Section VI.

## II. Theory

### General

The exposure of aluminum-gallium-arsenide lasers to gamma radiation from  $\text{Co}^{60}$  (~1.25 MeV) introduces defects in the material, in the form of vacancies and interstitials, which affect the performance of the lasers. These defects usually act as non-radiative recombination centers and, since they compete with the radiative centers for the injected carriers, they directly influence such performance parameters as power output, efficiency, and threshold current. Furthermore, if the defects are distributed inhomogeneously in the device, especially in the active region, some effect may be apparent in the output beam characteristics. An inhomogeneous distribution could result from the irradiation method or from device fabrication. Each area will be examined separately after a short description of the construction and operation of the injection laser.

### The Injection Laser

Prerequisites for the operation of a semi-conductor laser are a method to create a population inversion and a means to amplify radiation. The first requirement is met by using a heavily doped forward-biased p-n junction as shown in Fig. 1.

The application of a forward bias creates a narrow region containing both holes and electrons. Recombination occurs within this region with the emission of radiation. The condition for spontaneous emission has thus been created. Amplification occurs if radiation of energy near  $E_g$  travels through the region and stimulates the transition and if the population inversion is maintained by the injection of carriers.

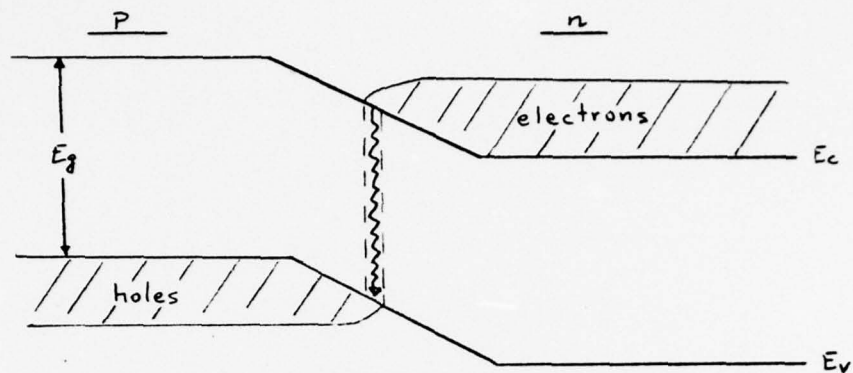


Fig. 1. Forward-Biased p-n Junction

A resonant cavity for the radiation is normally created by constructing the injection laser in the form of a Fabry-Perot cavity, that is, with parallel reflecting surfaces normal to the active region. Low injection current results in spontaneous emission and, as the current is increased, a point is reached where gains exceed losses and lasing action begins. This is expressed by Equation (1)

$$g = \alpha + \frac{1}{L} \ln (1/\sqrt{R_1 R_2}) \quad (1)$$

where  $g$  represents the gain per unit length,  $\alpha$  the losses per unit length,  $L$  the length of the cavity, and  $R_1$  and  $R_2$  are the reflectivities of the end surfaces.

Maximum gain occurs in the junction region where the population inversion exists, and radiation travelling through the device is confined to this region by changes in the dielectric constant, and hence in the refractive index of the material.

The injection lasers used in this investigation were stripe geometry, double-heterojunction devices, and were packaged as shown in Fig. 2.

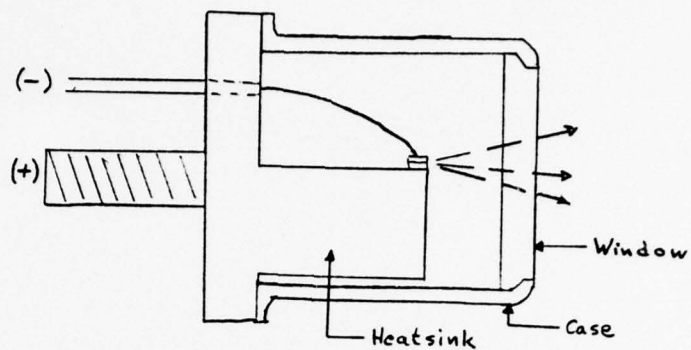


Fig. 2. Cross-Section of Laser Package

Details concerning device construction and composition were considered proprietary by the respective manufacturers and could not be obtained. However, a typical stripe geometry aluminum-gallium-arsenide laser may be constructed as illustrated in Fig. 3. The layers of a specific laser may be arranged differently, possibly including other layers as buffers or to assist in optical confinement.

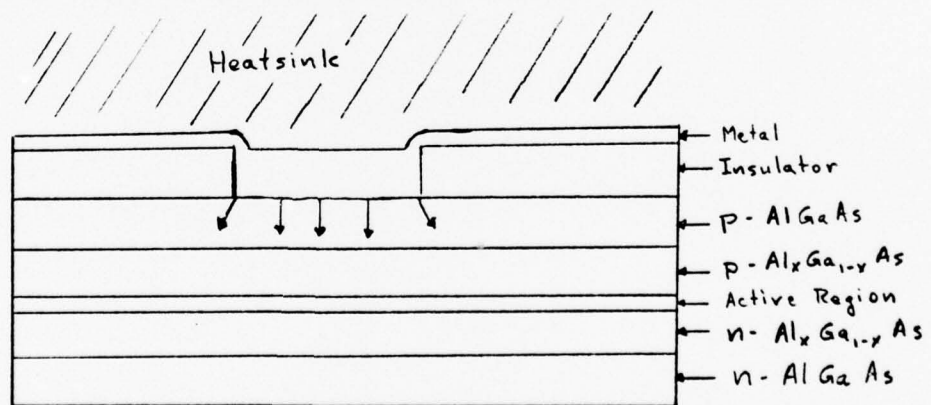


Fig. 3. Front View of Typical Stripe Geometry AlGaAs Injection Laser

The injection current is confined to a narrow region, as indicated by the arrows, emanating from the metallic "stripe" shown in Fig. 3.

Recombination occurs in the narrow active region and light is emitted in a fan shaped beam from one of the polished end surfaces.

#### Current Flow in the Injection Laser

The total current flowing across a p-n junction as in an injection laser consists of two components. One component, due to a diffusion process, results from carriers surmounting the barrier and recombining on the other side of the junction. The other, due to space charge region recombination (SCR), is due to carriers entering the depletion region and recombining there. The light output of the laser may be due to radiative recombinations resulting from one or the other of the components, or to a combination of both. That portion of the total current which results in radiative transitions is referred to as the *radiative current*.

The expressions for the diffusion current and the SCR current are presented as Equations (2) and (3).

$$I_D = \frac{qAD^{\frac{1}{2}}n_{po}}{\tau^{\frac{1}{2}}} \exp \frac{qV}{kT} \quad (2)$$

where  $q$  represents the electronic charge,  $A$  is the junction area,  $D$  is the electron diffusion coefficient,  $n_{po}$  is the minority carrier density,  $\tau$  is the carrier lifetime,  $V$  is the applied voltage,  $k$  is Boltzmann's constant, and  $T$  is the temperature.

$$I_{SCR} = \frac{qn_1wA}{2\tau} \exp \frac{qV}{2kT} \quad (3)$$

where  $n_1$  is the intrinsic carrier density and  $w$  is the width of the space charge region. The total current flow is normally due to a

combination of the two mechanisms, but, since SCR current increases faster than diffusion current as the energy gap widens, for comparatively large gap materials such as gallium-arsenide, the total current is normally given as  $I_{\text{tot}} \approx I_{\text{SCR}}$ .

Effect of Gamma Radiation on Current

Irradiation of aluminum-gallium-arsenide with gamma radiation introduces non-radiative recombination centers (Ref 3:4746). These non-radiative centers have the effect of decreasing the carrier lifetime,  $\tau$ . Since  $\tau$  is a factor in both current components, a change in  $\tau$  will result in a change in the current component. The total lifetime may be expressed as  $\frac{1}{\tau} = \frac{1}{\tau_R} + \frac{1}{\tau_{NR}}$ , where  $\tau_R$  and  $\tau_{NR}$  are, respectively, the radiative and non-radiative lifetimes. The introduction of non-radiative centers affects  $\tau_{NR}$  as illustrated by Equation (4)

$$\frac{1}{\tau_{NR}} = \frac{1}{\tau_{0NR}} + \sigma_{NRI} V_{th} N_{NRI} \quad (4)$$

where  $\tau_{0NR}$  is the pre-irradiation non-radiative lifetime,  $\sigma_{NRI}$  is the capture cross-section of the minority carriers,  $V_{th}$  is the thermal velocity, and  $N_{NRI}$  are the radiation induced non-radiative recombination centers.  $N_{NRI}$  can be replaced by  $C_I \phi$ , where  $C_I$  is the rate at which recombination centers are introduced with radiation,  $\phi$ . Equation (4) then becomes

$$\frac{1}{\tau_{NR}} = \frac{1}{\tau_{0NR}} + \sigma_{NRI} V_{th} C_I \phi \quad (5)$$

The use of Equation (5) allows the total carrier lifetime to be written as

$$\frac{1}{\tau} = \frac{1}{\tau_0} + \sigma_{NRI} V_{th} C_I \phi \quad (6)$$

where the subscript 0 denotes the pre-irradiation value.

The product  $\sigma_{NRI} V_{th} C_I$  is usually denoted by  $K$ , the damage constant. The effect of radiation on the total lifetime may therefore be written as

$$\frac{1}{\tau} = \frac{1}{\tau_0} + K\phi \quad (7)$$

Substitution of Equation (7) in the current equations results in expressions for  $I_D$  and  $I_{SCR}$  which contain the effect of radiation.

Equation (2) becomes

$$I_D = qAD^{\frac{1}{2}} n_{p0} \left( \frac{1}{\tau_0} + K\phi \right)^{\frac{1}{2}} \exp \frac{qV}{kT}$$

Upon simplification, this expression reduces to

$$I_D = I_{0D} (1 + \tau_0 K\phi)^{\frac{1}{2}} \quad (8)$$

where  $I_{0D}$  is the pre-irradiation diffusion current. Similarly, in the case of  $I_{SCR}$ ,

$$I_{SCR} = \frac{qn_i w A}{2} \left( \frac{1}{\tau_0} + K\phi \right) \exp \frac{qV}{2kT}$$

This simplifies to

$$I_{SCR} = I_{0SCR} (1 + \tau_0 K\phi) \quad (9)$$

As an example of the effect of radiation on the threshold current,  $I_{th}$ , consider a case where the total current flows predominantly by SCR, but light output is due to a diffusion component. Examination of

Equations (8) and (9) shows that the effect of radiation would be an effective reduction in the diffusion, or radiative, current component. Since the radiative component determines the threshold, total current would have to be increased until the diminished radiative component is increased to the point where lasing occurs.

#### Effects of Gamma Radiation on Power Output

Irradiation tends to decrease the optical output of an injection laser by introducing non-radiative recombination centers. The magnitude of the effect of radiation strongly depends on the radiative current flow mechanism in the device. The current flow mechanism, in turn, depends on the operating temperature, the applied voltage, and device construction related properties.

If the radiative current flow mechanism can be identified, the radiation induced change in output can be determined. A problem arises when a definite identification can not be made. This can occur when, at constant temperature and over a specific range of applied voltage, the radiative current flows by a combination of the mechanisms mentioned earlier. Methods available to identify the radiative current flow mechanism are discussed in the next sub-section.

Another factor influencing the measured change in output is the method used to perform the measurement. That is, results will differ depending on whether the measurement is performed at constant voltage or at constant current. A simple explanation for this effect is that at constant voltage additional carriers can be provided, while at constant current this is not possible.

The output of an injection laser may be expressed as

$$P = C \int_0^{\infty} n_p N_A dx \quad (10)$$

where C is a constant,  $n_p$  is the electron concentration on the p side,  $N_A$  is the acceptor concentration, and the integration is into the p region (Ref 2:176-177). If  $N_A$  is assumed to be of the form  $a \cdot x^n$ , where a is a constant and n is dependent on doping profile,  $n = 0$  for an abrupt junction and  $n = 1$  for a linearly graded junction, and  $n_p = n_{p0} \exp \frac{qV}{kT} \exp \left(-\frac{x}{L_e}\right)$  for the case of  $\exp \frac{qV}{kT} \gg 1$  (Ref 11:99), then Equation (1) can be written as

$$P = C n_{p0} a \exp \frac{qV}{kT} \int_0^{\infty} x^n \exp \left(-\frac{x}{L_e}\right) dx$$

where  $L_e$  is the electron diffusion length. Upon evaluation of the integral and substitution of  $L_e = \sqrt{D\tau}$ , this expression becomes

$$P = C n_{p0} a \exp \frac{qV}{kT} n! (D\tau)^{\frac{n+1}{2}} \quad (11)$$

Substitution of Equation (7) in Equation (11) yields, after simplification

$$\left(\frac{P_0}{P}\right)^{\frac{2}{n+1}} = 1 + \tau_0 K \phi \quad (12)$$

where  $P_0$  represents the pre-irradiation output. Equation (12) expresses radiation-induced change in a diffusion controlled output when measured at constant voltage.

If the measurement is performed at constant current, Equation (2) must be solved for V and the result substituted into Equation (11). Substitution yields, after simplification,

$$P = C_1 \tau \frac{n+2}{2} I_D$$

where the constants have been collected in  $C_1$ . Use of Equation (7) on this expression yields

$$\left(\frac{P_0}{P}\right)^{\frac{2}{n+2}} = 1 + \tau_0 K\phi \quad (13)$$

The total current in these devices, especially at low temperature and low supplied voltage, usually flows by SCR. Thus, to determine the change in output due to damage in the space charge region, the equation for total current is used, or  $I_{tot} \approx I_{SCR}$ . For a constant current measurement Equation (3) is solved for  $V$  and the result is substituted into Equation (11). The result is

$$P = C_2 \tau \frac{n+5}{2} I_{SCR}^2$$

The use of Equation (7) results in

$$\left(\frac{P_0}{P}\right)^{\frac{2}{n+5}} = 1 + \tau_0 K\phi \quad (14)$$

If the output is due to radiative recombination in the space charge region, then for a constant voltage measurement, the effect of gamma radiation is negligible. This is the case since the recombination rate through a particular type of center in the space charge region is controlled by the quasi-Fermi levels. These levels are affected by applied voltage and doping, but not by irradiation unless the amount of radiation is sufficient to cause a significant removal of carriers in the neutral regions.

### Determination of Current Flow Mechanisms

It has been indicated that radiation induced changes in output are dependent on the current flow mechanism responsible for the radiative transitions. The mechanisms of concern are diffusion and SCR.

A tentative identification of the current mechanisms can be made by examination of the P-V and I-V curves. Diffusion current may be written as  $I_D = C_1 \exp \frac{qV}{kT}$  and SCR current as  $I_{SCR} = C_2 \exp \frac{qV}{2kT}$ , where  $C_1$  and  $C_2$  are constants containing all the factors as given in Equations (2) and (3). Thus, if current is plotted versus voltage on a semilog graph, a slope of  $q/kT$  indicates a diffusion process and a slope of  $q/2kT$  indicates a SCR mechanism. When current is plotted versus voltage, the values of current represent the total current. Similarly when output is plotted versus voltage, the slope of the curve gives an indication of the current flow mechanism responsible for the radiative transitions.

A further means of identification is due to the differing effects of radiation on diffusion controlled and SCR controlled output. The effect of radiation on diffusion output is much more pronounced than on SCR output. Comparison of the pre-irradiation P-V curve with the post-irradiation P-V curve may, over a range of V, show a significant difference, indicating diffusion controlled output, or may show only a slight change, indicating SCR controlled output.

### Shift of Emission Peak

A shift in energy of the emission peak may occur with a change in the applied voltage. If this happens it is an indication of the presence of a radiative current due to a tunneling mechanism. Tunneling probability is highest near the respective quasi-Fermi levels of

the carriers (Ref 7:186). The level separation is directly dependent on V. Thus, a change in applied voltage causes a change in level separation and a photon emitted as a result of a tunneling process reflects this energy shift. The tunneling current may be expressed as

$$I_{\text{tun}} = B \exp(\alpha_t V) \quad (15)$$

where B is a constant containing dopant concentration and  $\alpha_t$  depends on the shape of the junction and also contains dopant concentration. The only radiation-sensitive quantity in Equation (15) is the dopant concentration. This means that a radiation induced change in the tunneling current only becomes evident when the amount of radiation is sufficient to remove a significant number of carriers by effectively changing the dopant concentration. Share, et al. invoked the concept of the luminescent killer center to explain the peak shift with irradiation. Assuming donor-acceptor pair radiative transitions, the shift to higher energies can be explained if the more distant pairs are removed from the radiative process by the killer centers.

#### Radiation Induced Beam Changes

The shift of the emission peak with irradiation has just been discussed. Changes in the axial mode structure of the emitted light are not anticipated since these modes are not determined by any radiation sensitive quantities. Changes in the transverse modes could occur if radiation affected the properties of the active region. Transverse mode separation is given by

$$\Delta\lambda/\Delta m = -\lambda^2/2\pi n_e x_0 \quad (16)$$

where  $n_e$  is the wavelength dependent index of refraction and  $x_0$  represents a constant which measures the rate of decrease of the index of refraction either parallel or perpendicular to the junction, depending on which case is considered (Ref 11:711). The effect of radiation on the wavelength is minimal, but the introduction of non-radiative recombination centers may change the wave-guiding properties of the cavity. This effect would be represented by a change in the product of the effective refractive index and the index rate of change. A change in the wave-guiding characteristics of the cavity would appear as changes in the intensity distribution of the beam and in changes in beam divergence.

### III. Description of Samples and Experiments

The injection lasers used in this study were type C30127 from RCA, and type LCW-10 from Laser Diode Laboratories, Inc. Both types were designed to operate in the continuous wave mode at room temperature. Relevant performance characteristics, as provided by the manufacturers, are given in Table I. Specific information was provided with each sample and is listed in Table II. Detailed information about the AlGaAs lasers was considered proprietary by the respective manufacturers and could not be obtained.

Table I

Typical Operating Characteristics at Room Temperature  
as Provided by Manufacturer

Parameter	LCW-10	C30127	Units
$P_o(\text{max})$	14	<15	mW
$I_{th}$	200	250	mA
Emission Peak	850	820	nM
Beam Spread			
Parallel	5	5	deg, HWHM
Perpendicular	20	20	deg, HWHM

Table II

Specific Information Provided by Manufacturer

Type	Sample	$I_{th}$ (mA)	$I_{max}$ (mA)	$P_o$ (mW)
LCW-10	1	180	230	11.6
LCW-10	2	210	260	12.5
C30127	66	240	500*	5 at 260mA
C30127	68	210	500*	5 at 245mA

\* $I_{max}$  provided as 500mA for all type C30127 samples.

Initial measurements were performed at room temperature prior to irradiation to verify the manufacturer's data. Then the initial experiments were repeated at liquid nitrogen temperature since post-irradiation measurements were to be conducted at that temperature.

Pre-irradiation experiments determined the I-V and P-V relationships, the intensity distribution in the beam and the divergence, the spectral distribution at various, arbitrarily selected forward currents, and the emission peak shift as a function of applied voltage. Additionally, output, power efficiency, differential external quantum efficiency, and threshold current information were obtained.

To obtain the I-V and P-V information at room temperature, the circuit depicted in Fig. 4 was used.

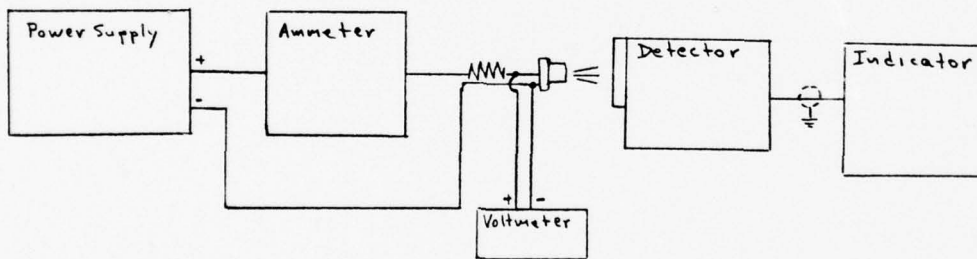


Fig. 4. Circuit for Measuring I-V, P-V Relationships

The laser device was attached to a heat sink capable of dissipating 2 Watt and a resistor, R, was placed in the circuit to eliminate current spikes (14 $\Omega$ , 10W). The injection current was provided by a Trygon Electronics Model DL 40-1 power supply and was measured with a Honeywell Digitest Model 333. The voltage across the device was also measured with a Model 333. The laser was centered at a distance of 1.5cm from

the input aperture of the EG & G Model 580-11A Detector and the laser output was displayed by the Model 580-11A Indicator Unit.

Data were obtained by adjusting the power supply to a specific current, as presented by the ammeter, noting the corresponding voltmeter reading and the detector current displayed by the indicator unit. After each reading the power supply output was reduced to zero to avoid heating effects.

The values obtained were readily converted to power supplied ( $I_F \times V$ ), power output of the laser (detector current x constants supplied with Model 580-11A radiometer), and power efficiency (ratio of the powers). Additionally the P-V, I-V, and P-I relations could be plotted. The threshold currents could then be obtained from the P-I plots.

The combination of heat sink and reduction of the output of the power supply to zero between readings kept the temperature at each individual reading within 1°C of room temperature. The heat sink alone allowed a rise of 2-3°C above room temperature at forward currents ~50% above threshold when power was applied continuously for a period of approximately five minutes.

Intensity distribution was obtained by mounting the laser on a moveable carriage at a fixed distance, in the far field, from the detector head input plane and illuminating a 0.5mm hole. The position dependent angle was then calculated and related to the laser output as represented by the detector current. Again, the power supply output was reduced to zero between readings. Laser output was then plotted against the calculated angle and the beam divergence in degrees at the 50 percent points was read from the plot.

To obtain spectral information a configuration as shown in Fig. 5 was used.

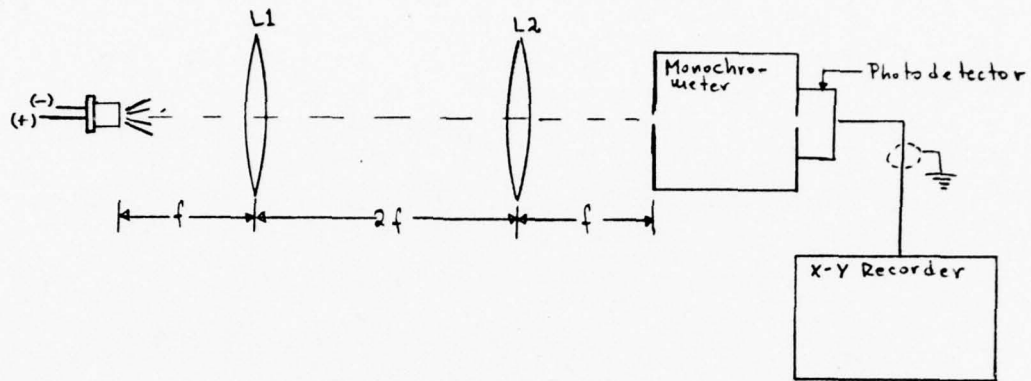


Fig. 5. Configuration for Obtaining Spectral Data

Lenses 1 and 2 were identical (dia = 3cm,  $f = 50.8\text{mm}$ ) and focussed the laser light on the entrance slit of the .25m Ebert monochromator. A Si photodetector (HAV1000) was attached to the exit slit and provided the input for the H-P/Moseley Model 7001 X-Y Recorder. Best results, in terms of resolution, were obtained with the smallest available slits, 25mm. The circuit shown in Fig. 4 was used and the laser was operated at arbitrarily selected forward currents above threshold. The system was aligned by using an IR detector plate to focus the light on the entrance slit and by monitoring the pen deflection of the recorder. When necessary, neutral density filters were used immediately in front of Lens 2 to reduce the input to the photodetector. The spectral plots were obtained by selecting an appropriate starting point for the scan, adjusting recorder sensitivity and scan speed, adjusting the power supply to the desired forward current, and simultaneously activating monochromator and recorder scan.

As stated, these measurements were then repeated at liquid nitrogen temperature. In this case, the samples were attached to a glass rod and were totally immersed in the liquid. The experimental configuration was the same as described above, except that the laser output had to penetrate the double walls of the dewar. Since this study was concerned with relative effects, this was not considered to present a problem. As at room temperature, the power supply was returned to zero between readings.

The samples were irradiated by placing them in the exposure chamber of a  $\text{Co}^{60}$  source for the length of time required to absorb a predetermined dosage. The orientation of the samples in the chamber was random. Exposures to  $10^7\text{Rad}(\text{Si})$  were accomplished at the Air Force Institute of Technology's Nuclear Center, and exposure to  $10^8\text{Rad}(\text{Si})$  was conducted at the Gamma Irradiation Facility of the Sandia Laboratories.

Initially only one sample was irradiated to  $10^4\text{Rad}(\text{Si})$  to observe the severity of the effects. After analyzing performance changes, the same sample was irradiated to  $2 \times 10^4$  and  $5 \times 10^4\text{Rad}(\text{Si})$ , with measurements being taken after each exposure. Only then, after having obtained a general idea of radiation induced degradation, were the other samples irradiated to  $10^4\text{Rad}(\text{Si})$ . Since samples 66 and 68 exhibited a rapid drop in performance, they were irradiated to  $10^5$ ,  $5 \times 10^5$ , and  $10^6\text{Rad}(\text{Si})$  by increments of powers of 10. The intermediate levels were not thought necessary for samples 1 and 2 since they showed no decrease in performance after the first exposure. Irradiation was accomplished at room temperature; subsequent measurements at  $77^\circ\text{K}$ .

#### IV. Results and Discussion

##### General

The results of the different measurements are presented and discussed separately. Factors influencing the accuracy of the measurements are considered in each case, and, when possible, the measured effect has been attributed to the responsible physical mechanism.

##### Pre-Irradiation Performance

The measured values of the threshold current,  $I_{th}$ , the output power,  $P$ , and the position of the emission peak are listed in Table III for comparison with the data provided by the manufacturers. The temperature of the laser case,  $T_c$ , at which the measurements were performed, is also given.  $I_{th}$  was determined by extrapolating the linear portion of the I-P curve to the I axis. This method of obtaining the values of  $I_{th}$  may partially account for the difference between the manufacturers' and measured values. Another factor to account for the difference could be the temperature of the measurements. Temperature strongly affects  $I_{th}$  and it was not known at what specific value of "room temperature" the manufacturers performed their measurements.

Temperature also affects the output power and may be one of the causes of the difference. Errors in the power due to equipment and procedure are limited to plus or minus six percent of the values given. The emission peak position was obtained by placing an envelope over the emission spectrum and using the highest point. In view of the limitations of the equipment used for this measurement, the given values of the emission peaks must be considered as representative only, rather than as absolute.

Table III

## Measured Pre-Irradiation Characteristics at Room Temperature

Type	Sample	$I_{th}$ (mA)	P(mW) at I(mA)	$T_c$ (°K)	Emission Peak (nm)
LCW-10	1	165	12.6 at 230	296	883
LCW-10	2	195	11.8 at 260	297	884
C30127	66	235	6.9 at 260	294	819
C30127	68	240	1.6 at 245	296	821

The same measurements, performed at liquid nitrogen temperature, resulted in the values given in Table IV.

Table IV

## Measured Pre-Irradiation Characteristics at 77°K

Type	Sample	$I_{th}$ (mA)	P(mW) at I(mA)	Emission Peak (nm)
LCW-10	1	60	44.2 at 200	829
LCW-10	2	70	51.2 at 200	839
C30127	66	30	81.1 at 200	764
C30127	68	30	31.3 at 200	768

All samples except number 66 presented smooth I-P curves. Sample 66 exhibited a "kink" at room temperature and at 77°K. This "kink" has been explained as due to unstable horizontal modes (Ref 6:659-660) and cavity competition (Ref 4:687-691). Additionally, each sample exhibited an apparent shift of emission peak with applied voltage, indicating the presence of a tunneling mechanism (Ref 7:186). Shift of emission peak with applied voltage is shown in Figs. 6 and 7.

The intensity distribution and divergence were measured in the far field at room temperature only. The pre-irradiation values of the beam divergence were found to agree closely with those given by the

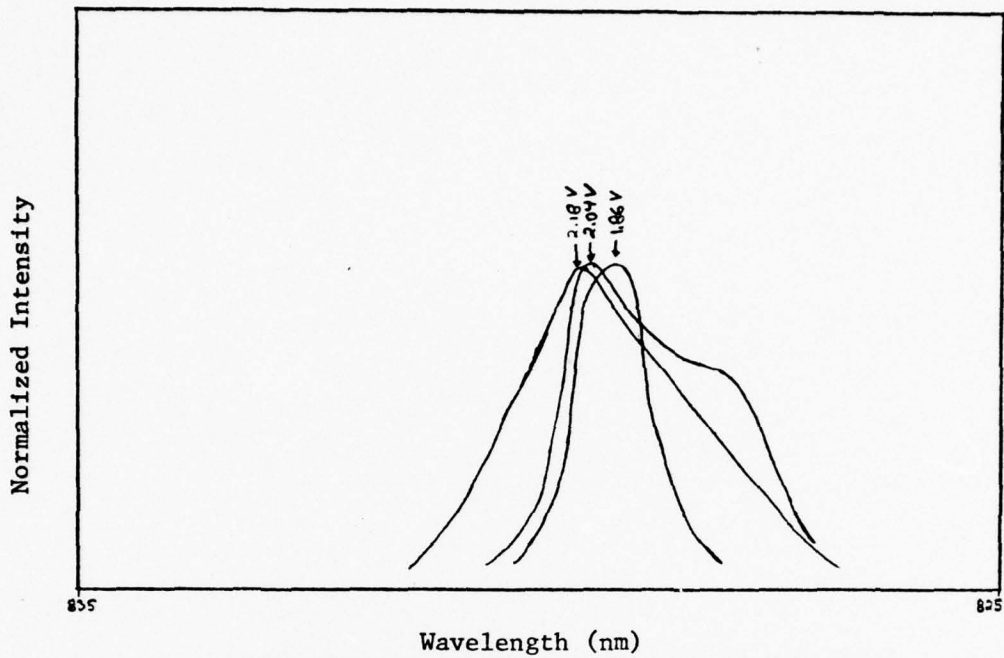


Fig. 6a. Shift of Emission Peak with Applied Voltage at 77°K, Pre-Irradiation, Sample 1

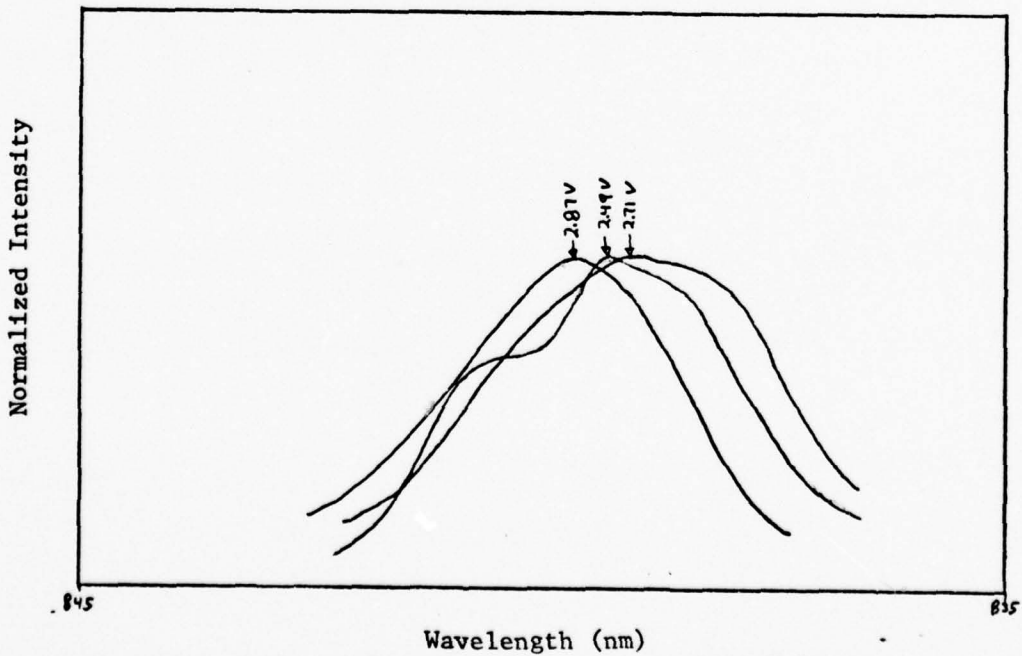


Fig. 6b. Shift of Emission Peak with Applied Voltage at 77°K, Pre-Irradiation, Sample 2

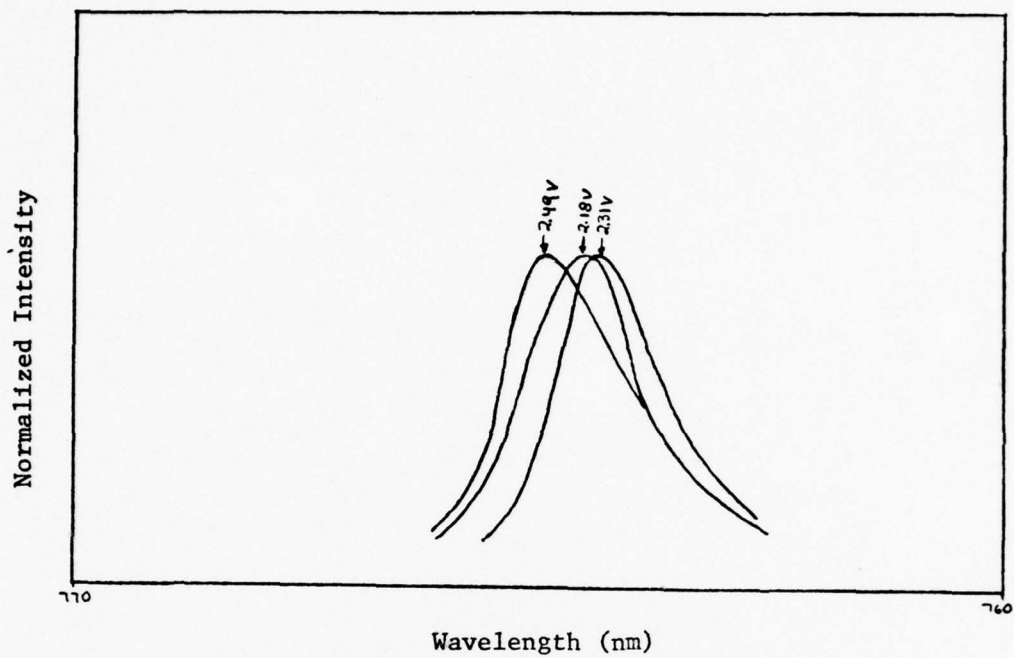


Fig. 7a. Shift of Emission Peak with Applied Voltage at 77°K, Pre-Irradiation, Sample 66

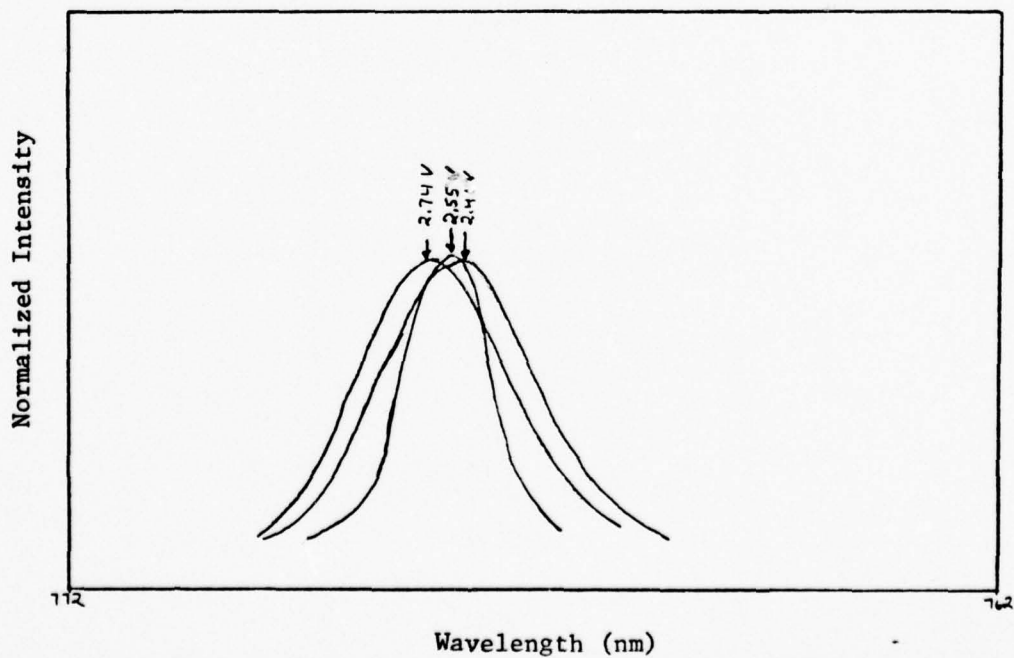


Fig. 7b. Shift of Emission Peak with Applied Voltage at 77°K, Pre-Irradiation, Sample 68

manufacturers. Pre- and post-irradiation intensity distributions are presented together later for comparison purposes.

The I-V and P-V curves for four samples are shown in Figs. 8a and 8b. The differences in slope between the output and current curves are readily apparent, indicating different mechanisms for the total and radiative current flow. The bending of the output curves at higher values of V should be noted. It could be due to the expected increase in resistive losses, or to a change in the radiative current flow mechanism.

The information used to generate the I-V and P-V curves was also used to plot power efficiency. Power efficiency is defined as the ratio of the output power and the supplied power, or  $P_{out}/IV$ . The power efficiencies for the samples are shown in Figs. 9a and 9b.

#### Measured Effect of Radiation on Threshold Current

As stated earlier, the initial exposure of the samples was to  $10^4$ Rad(Si). Subsequent exposures raised the dosage to  $10^8$ Rad(Si).  $I_{th}$  was determined from the I-P curves as before. Figs. 10a - d present the current-output relationships for the different levels of irradiation, and Table V gives the values of the threshold current as a function of dosage within plus or minus five percent.

The effect of radiation on the threshold current differed significantly between the two types of samples.  $I_{th}$  of samples 1 and 2 did not change noticeably with irradiation, whereas samples 66 and 68 reacted in accordance with the predictions of Section II. Possible explanations for the observed results are included in the next subsection.

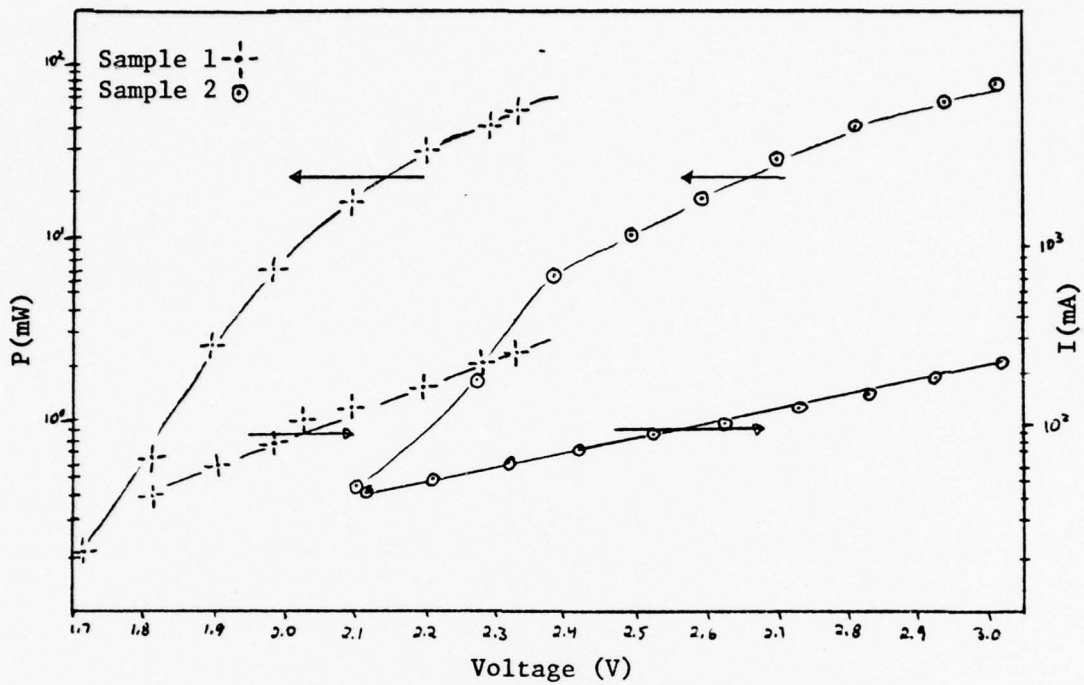


Fig. 8a. Pre-Irradiation Power-Voltage and Current-Voltage Relation at 77°K

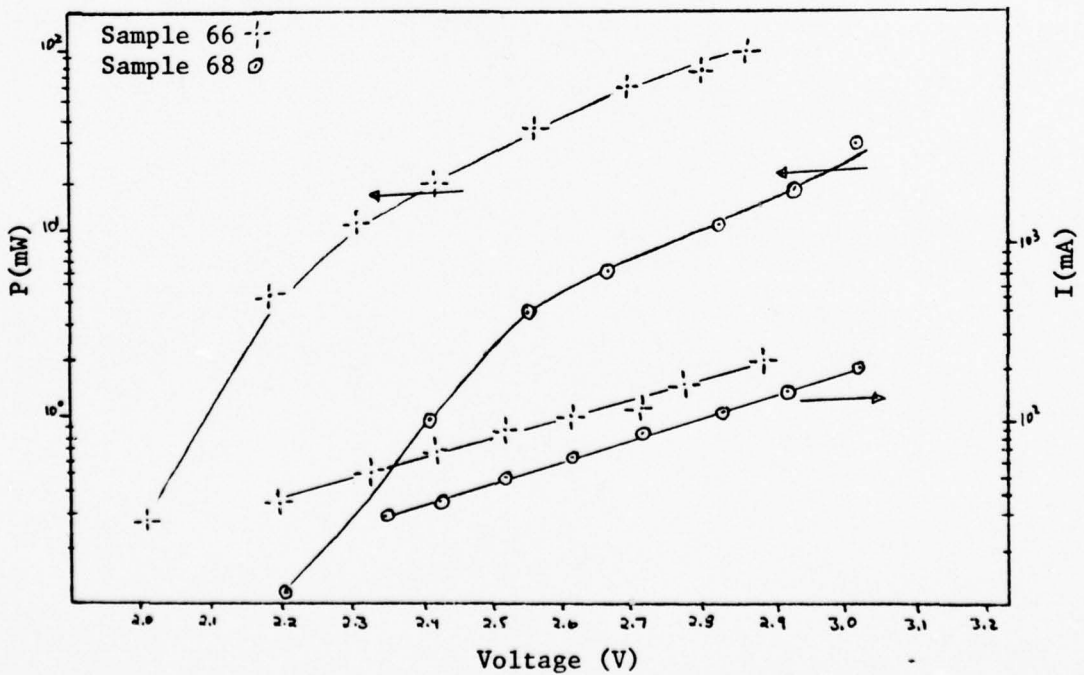


Fig. 8b. Pre-Irradiation Power-Voltage and Current-Voltage Relation at 77°K

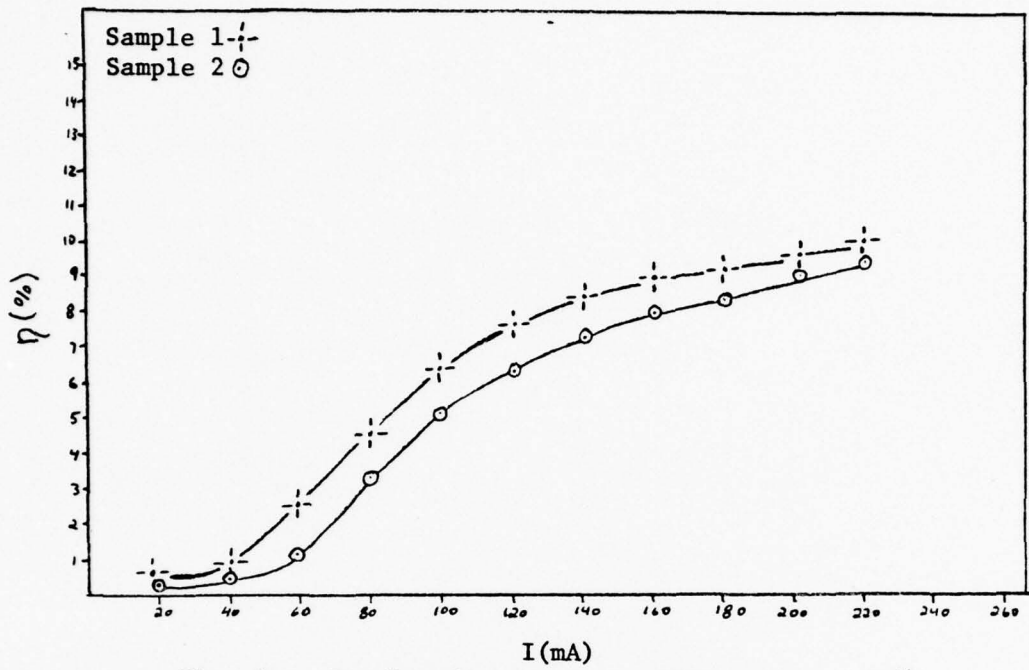


Fig. 9a. Pre-Irradiation Power Efficiency at 77°K

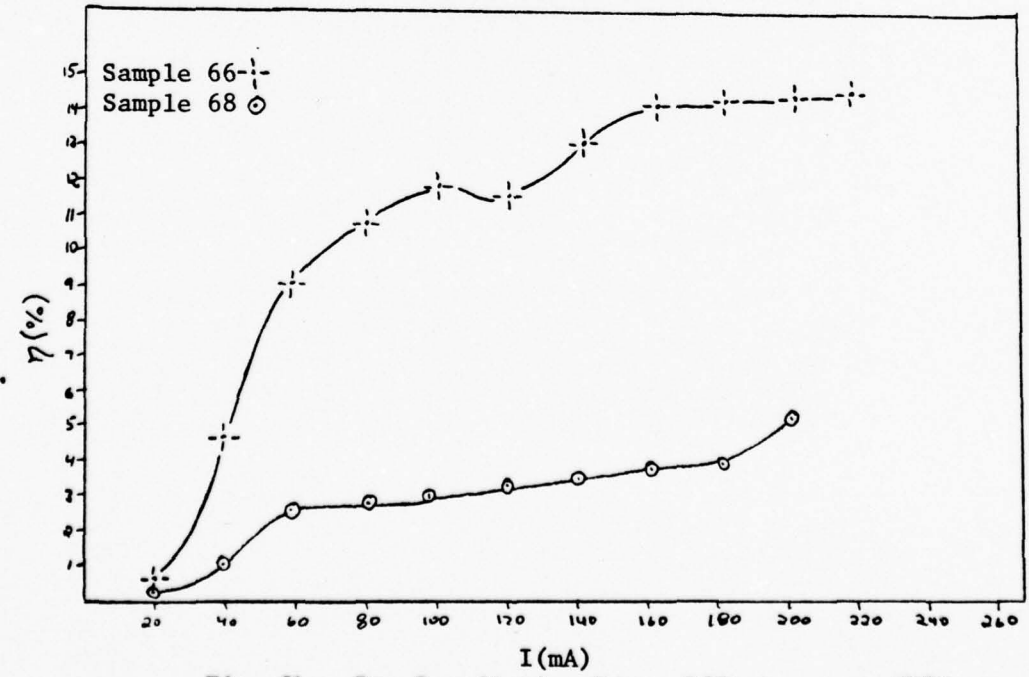


Fig. 9b. Pre-Irradiation Power Efficiency at 77°K

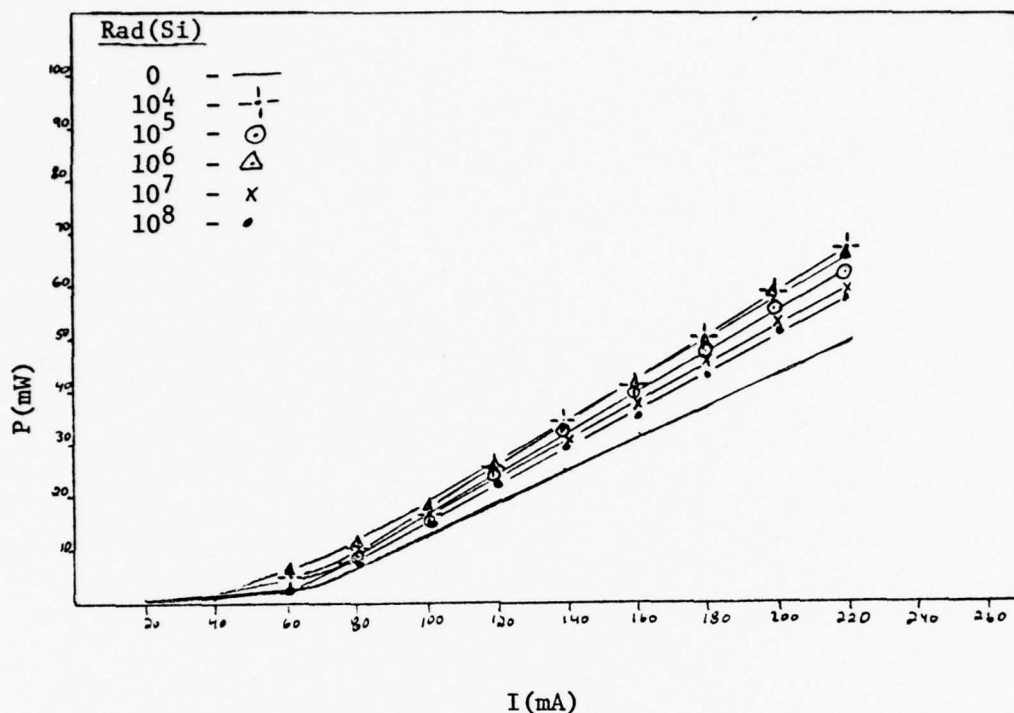


Fig. 10a. Power-Current Relation as Function of Dosage at 77°K, Sample 1

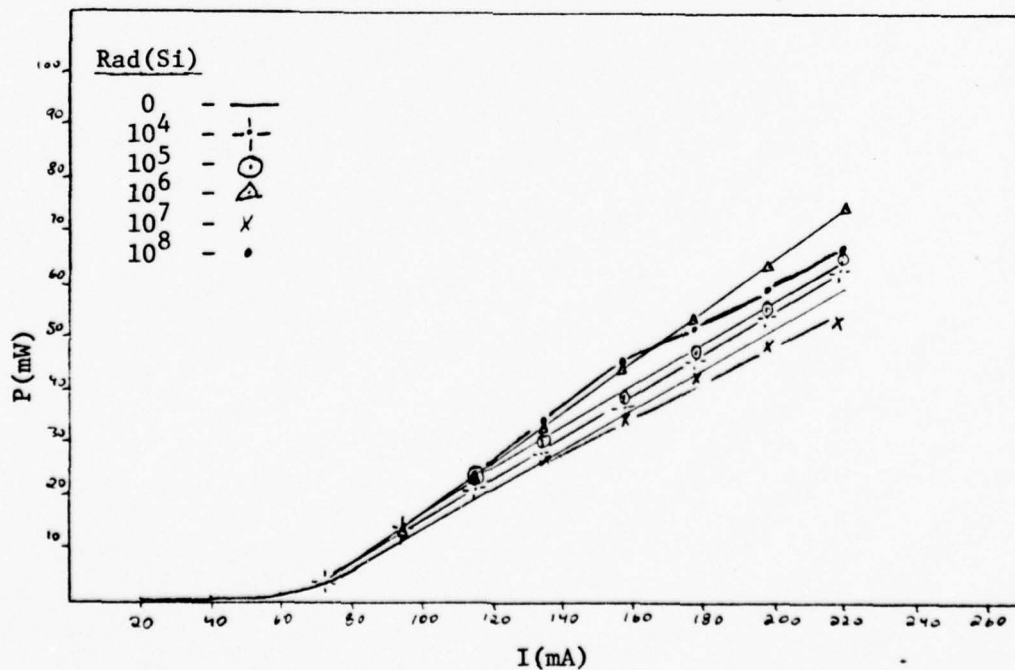


Fig. 10b. Power-Current Relation as Function of Dosage at 77°K, Sample 2

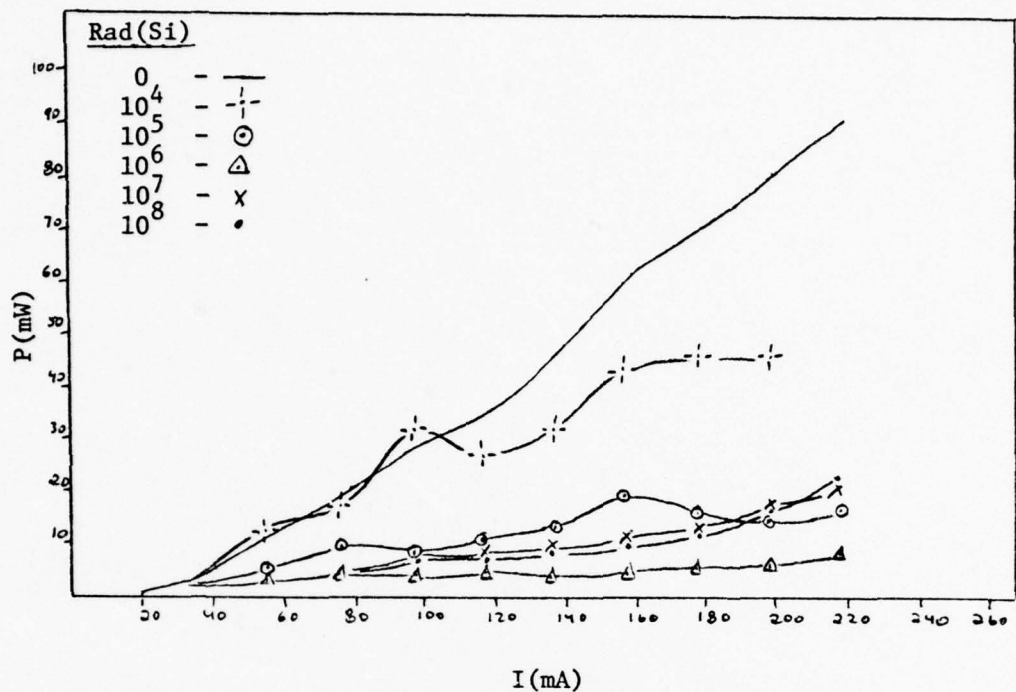


Fig. 10c. Power-Current Relation as Function of Dosage at 77°K, Sample 66

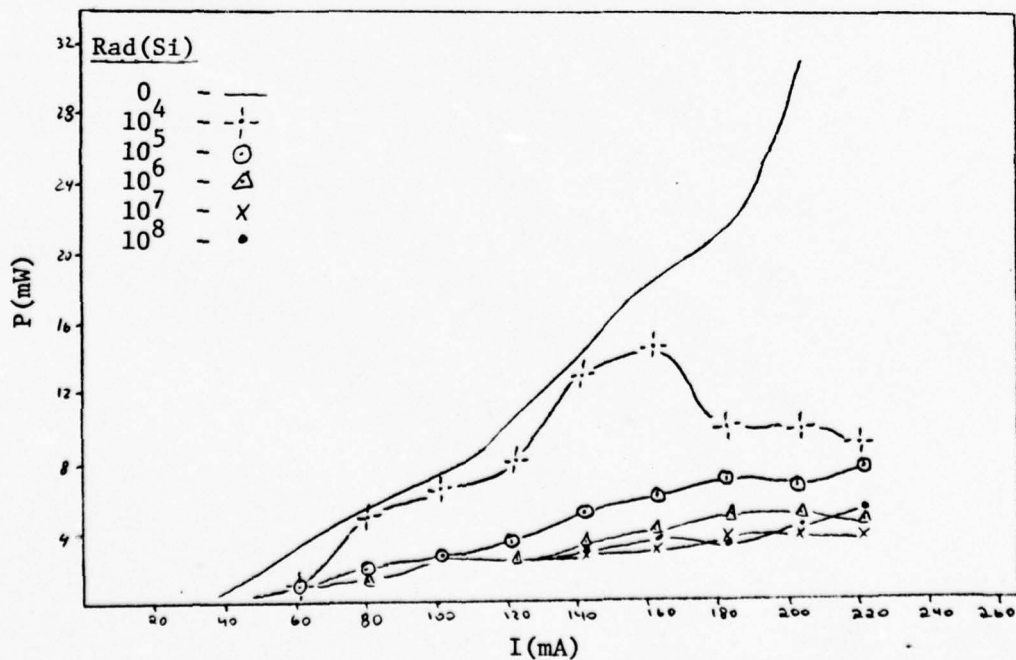


Fig. 10d. Power-Current Relation as Function of Dosage at 77°K, Sample 68

Table V

## Threshold Current as Function of Dosage

Sample Rad(Si)	1 $I_{th}$ (mA)	2 $I_{th}$ (mA)	66 $I_{th}$ (mA)	68 $I_{th}$ (mA)
0	60	70	30	30
$10^4$	60	70	35	35
$10^5$	60	70	35	70
$10^6$	60	70	<40*	~100*
$10^7$	60	70	<40*	>100*
$10^8$	60	70	<60*	>100*

\*Spectral data used in conjunction with I-P plot

Measured Effect of Radiation on Power Output

For comparison with the measured pre-irradiation output shown in Table IV, the output as a function of dosage at constant current is presented in Table VI.

Table VI

## Post-Irradiation Power Output at Specific Forward Currents

Sample Rad(Si)	P(mW) at I = 200 mA			
	1	2	66	68
0	44.2	51.2	81.1	31.3
$10^4$	59.9	54.8	43.6	9.7
$10^5$	57.6	56.7	14.0	6.2
$10^6$	59.9	63.7	4.6	4.6
$10^7$	55.1	49.6	14.0	3.5
$10^8$	52.8	57.6	14.2	3.8

While the data for Samples 1 and 2 is representative of the I-P relationship over the range of I, this is not the case for Samples 66 and 68 (see Fig. 11a - d). The data in Table VI show the increase in output for Samples 1 and 2 to  $10^6$ Rad(Si) and the drastic decrease in the case of Samples 66 and 68.

Theoretical considerations showed the possibility of comparative radiation hardness, but none of the principles advanced can explain the observed performance increase of Samples 1 and 2. A device containing radiative recombination centers in the space charge region, a step doping profile, and heavy doping would be expected to be quite radiation resistant. Radiative recombination in the space charge region is quite resistant to irradiation; a step profile reduces  $n$  to zero in the equations relating power to dosage; and the effect of any introduced non-radiative centers would be comparatively minor at moderate dosage if, in the pre-irradiated device, the number of radiative centers were much larger than the number of non-radiative centers. A possible explanation for the increase in power output may be that some of the radiation induced defects act as radiative recombination centers in the LCW-10 diodes. This effect has not been noticed in GaAs, but has been observed in SiC light emitting diodes (Ref 10:239).

The rapid drop in performance of Samples 66 and 68 possibly may be attributed to device construction. Rapid deterioration would be experienced if the device was only lightly doped so that the introduction of non-radiative centers would have a relatively large effect. Additionally, higher sensitivity to radiation is predicted by the theory for a diffusion controlled output and a linear radiative center profile ( $n = 1$ ). If the concept of the luminescent killer center is added to the above factors, the rapid degradation of Samples 66 and 68 is explained.

The lack of change in the threshold current of the type LCW-10 samples verifies the assumption that any introduction of non-radiative

recombination centers is offset. The behavior of the threshold current in the type C30127 samples generally adheres to the theory presented. For both samples of this type the output decreased rapidly with dosage and "flat" I-P curves resulted.

The data of Table VI do not reflect losses incurred due to the walls of the dewar, nor are they corrected for the small amount of radiation missing the detector head input plane. The experimental configuration was such that any radiation within a  $\sim 114$  degree cone would hit the detector. Equipment allowed for an error of plus or minus six percent. Fixed losses as presented by the dewar were not considered important since the interest was on radiation induced changes rather than on absolute values.

#### Power Output-Voltage, Current-Voltage, and Damage Factors

Output versus voltage plots are presented for all samples combining the pre-irradiation curve with the curve after  $10^8$ Rad(Si). Simultaneously shown are the pre-irradiation and  $10^8$ Rad(Si) current-voltage curves. Examination of Figs. 11 through 14 reveals that the I-V characteristics of all samples are relatively unaffected by irradiation, showing only a slight shift to higher voltage for constant current. The effect on the P-V curves is more dramatic, and, as expected, differs significantly between the two types of diodes. Type LCW-10, shown in Figs. 11 and 12, exhibits a moderate decrease in output at lower voltages where a portion of the radiative current may be attributed to a diffusion mechanism. At higher voltages it appears that a SCR mechanism becomes dominant since the output remains relatively unaffected by irradiation.

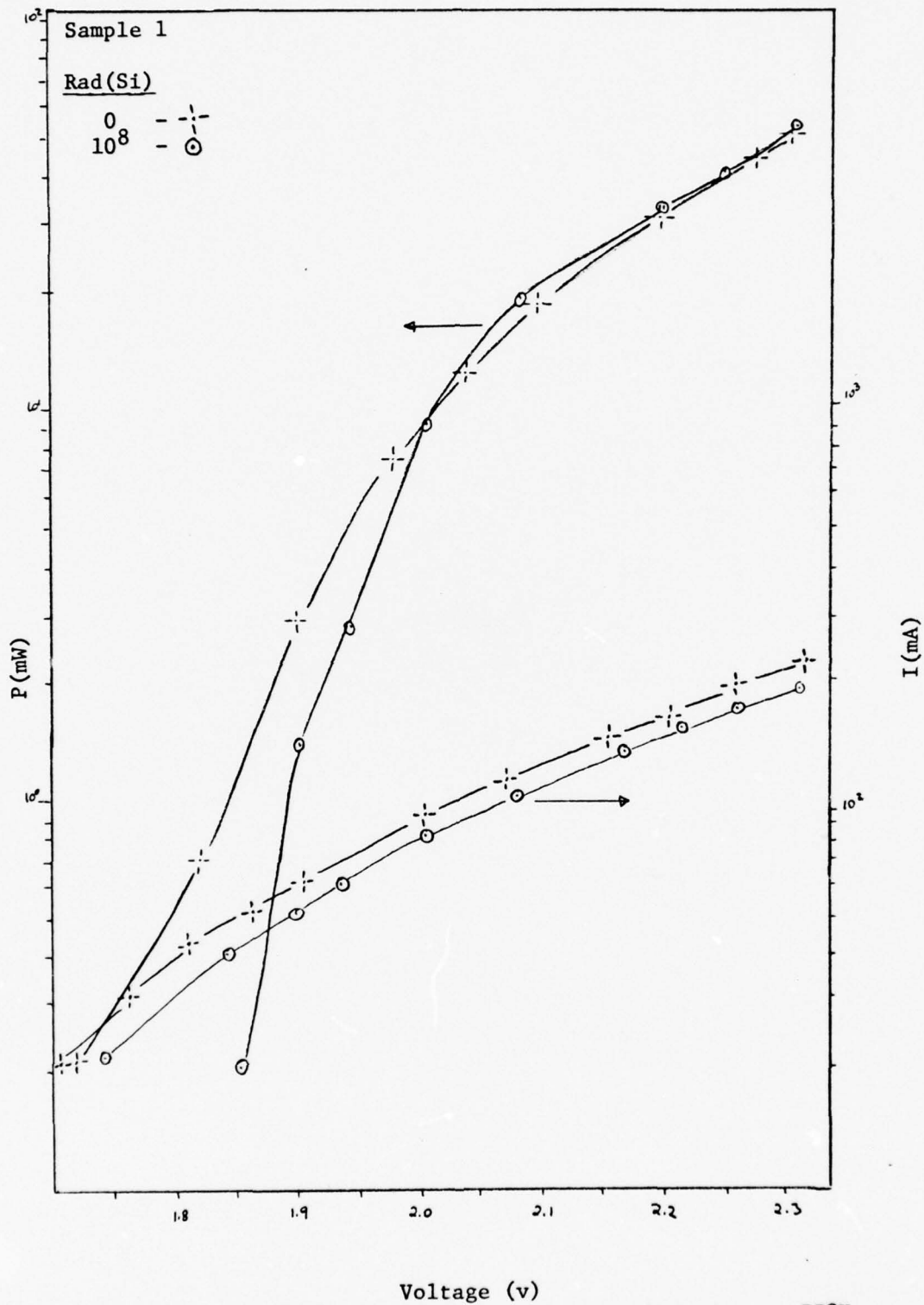


Fig. 11. Power-Voltage and Current-Voltage Relation at 77°K, Pre- and Post-Irradiation

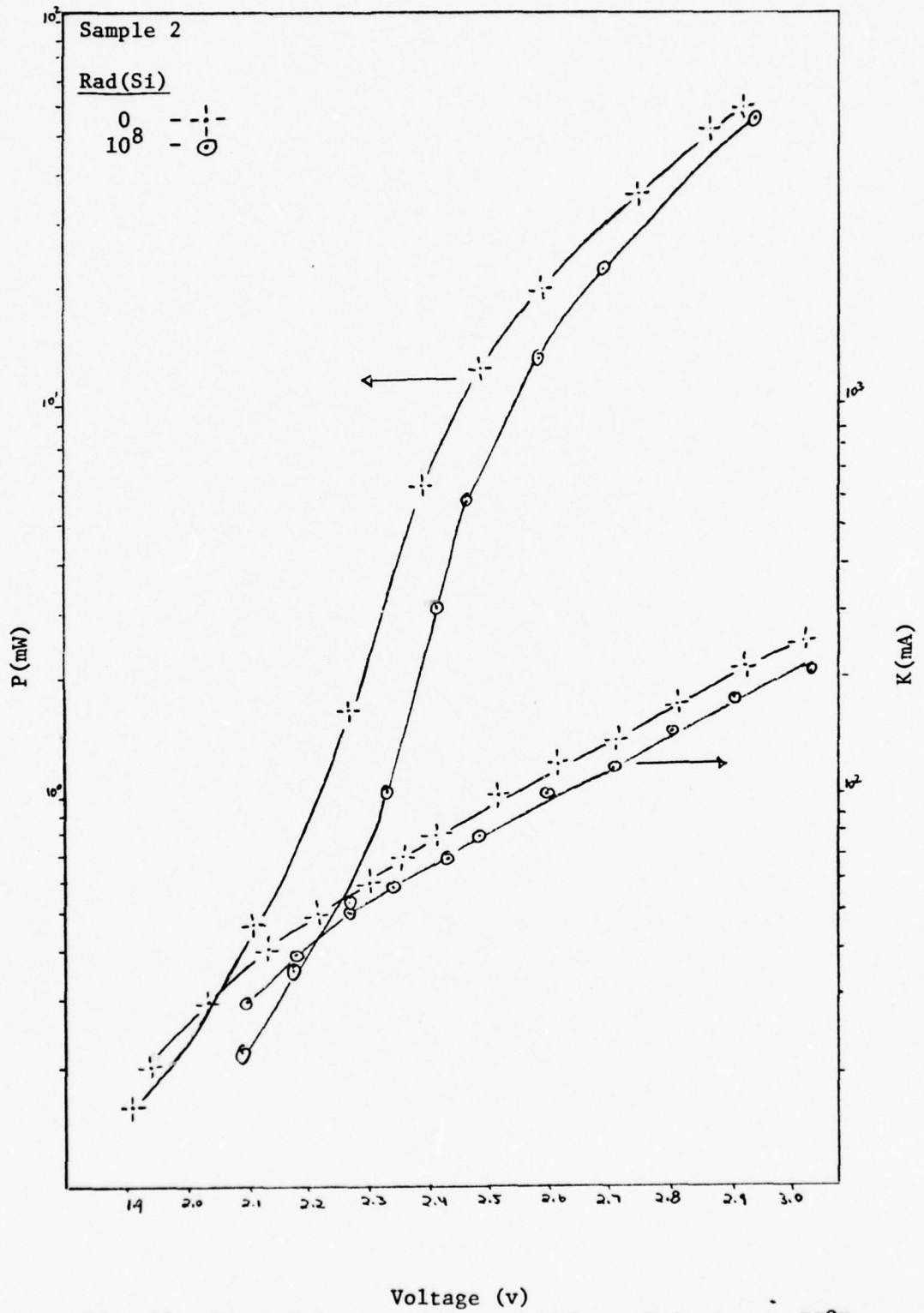


Fig. 12. Power-Voltage and Current-Voltage Relation at 77°K, Pre- and Post-Irradiation

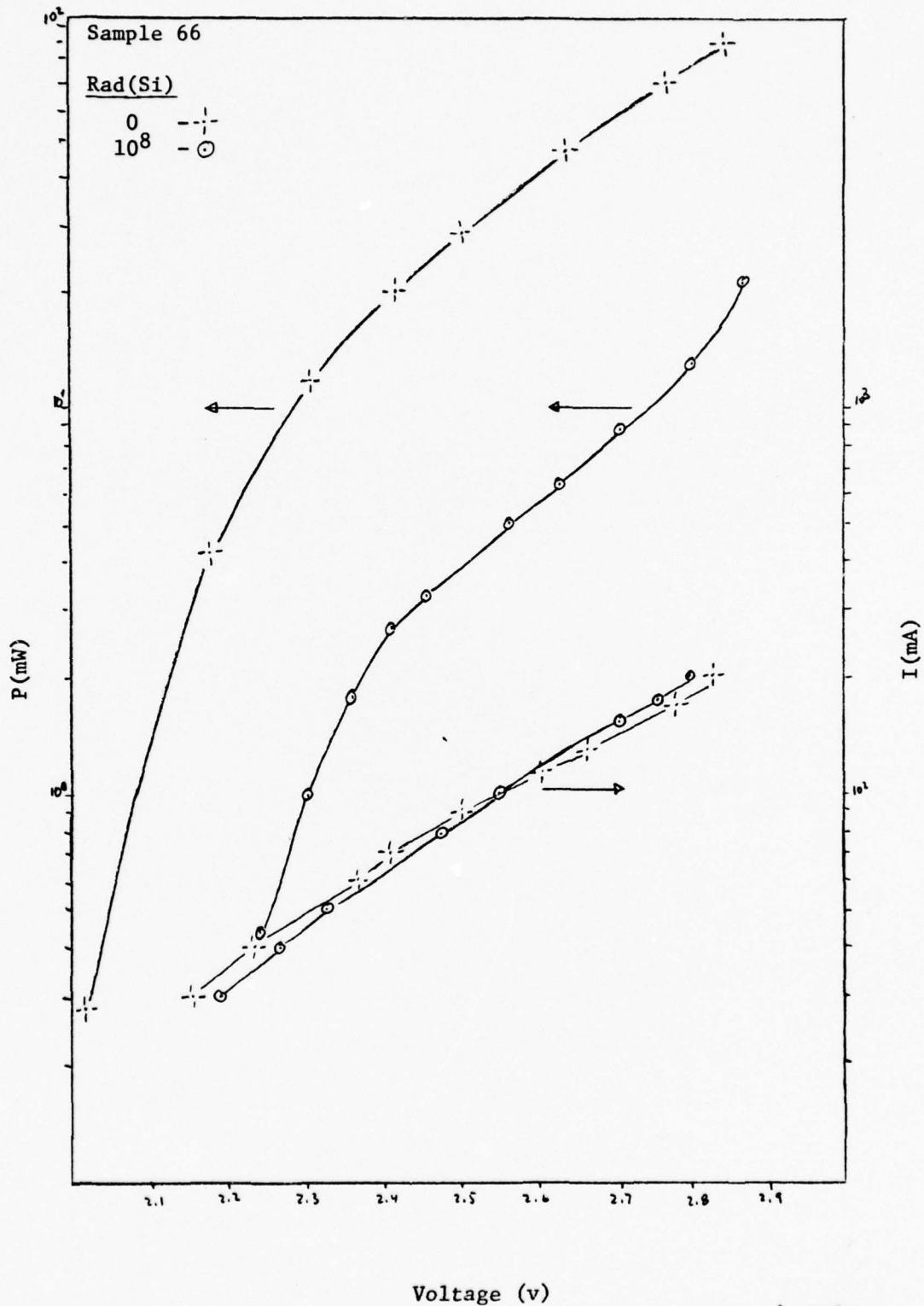


Fig. 13. Power-Voltage and Current-Voltage Relation at 77°K, Pre- and Post-Irradiation

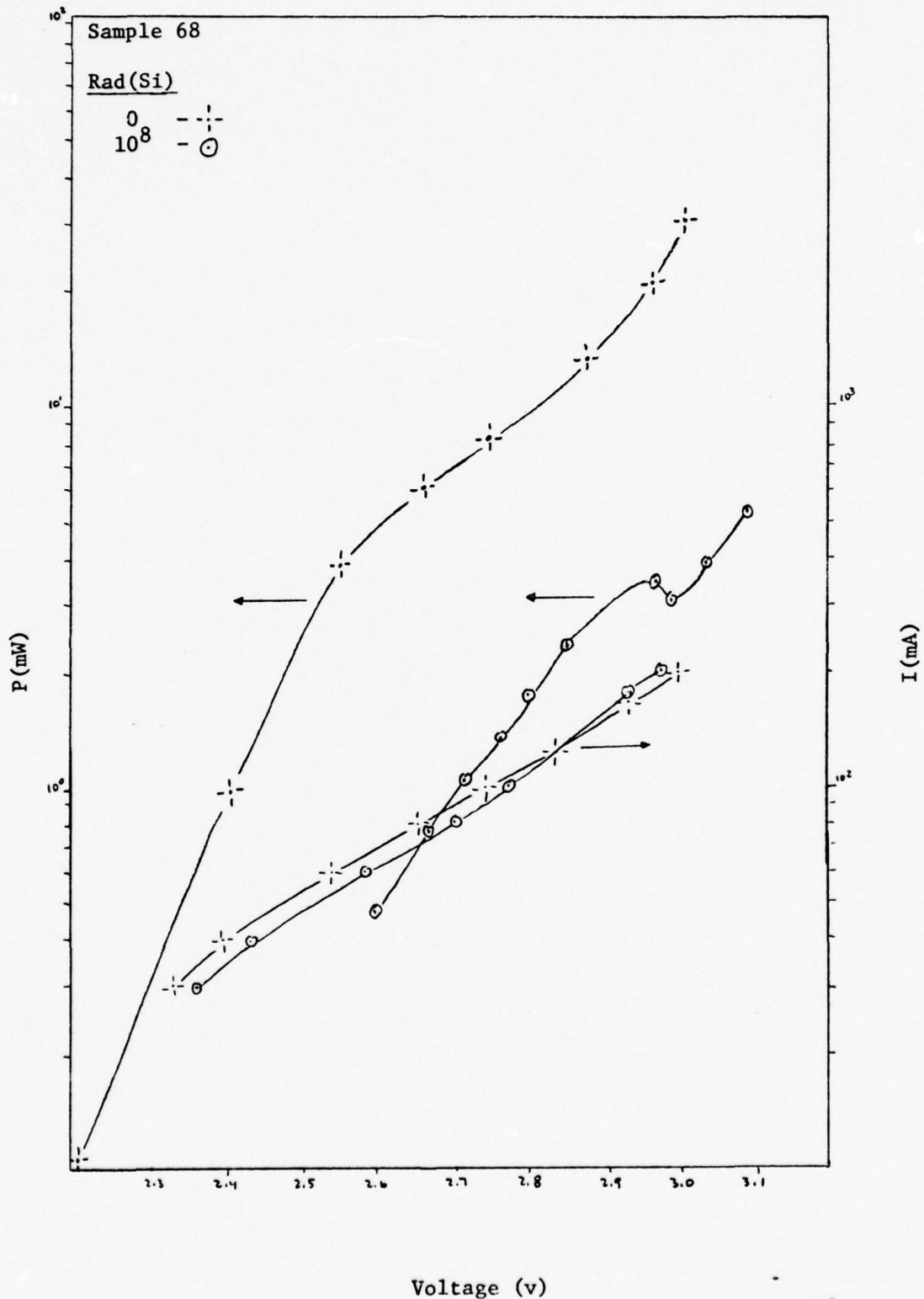


Fig. 14. Power-Voltage and Current-Voltage Relation at 77°K, Pre- and Post-Irradiation

The behavior of type C30127, Figs. 13 and 14, is quite different. The large decrease in output over the whole voltage range measured indicates that a diffusion mechanism remains dominant. A possible explanation for this behavior may be the relative absence of radiative recombination centers in the space charge region. The bending of the P-V curves at higher values of V may at least partially be attributed to increasing resistive losses, although in the case of type LCW-10 the changing radiative current mechanism has an effect.

Since spectra were obtained at constant current, a radiation induced shift in the emission peak may be explained, to some extent, by the changed I-V characteristics. At constant current irradiation caused a slight increase in voltage. If a tunneling mechanism is responsible for some of the output, then the change in voltage would cause a shift in emission through its effect on the quasi-Fermi levels.

The data used to generate Figs. 11 through 14 also allows calculation of the constant voltage and constant current damage factors. This information is presented in Figs. 15a - d. Note again the almost exponential decrease in the case of Samples 66 and 68. This behavior reinforces the concept of the luminescent killer center which removes a number of radiative centers from the radiative process. Values of  $\tau_0 K$  have been calculated and are presented in Table VII.

Table VII

Calculated Damage Factors,  $\tau_0 K$

Mechanism Sample	Diffusion, $\tau_0 K(\text{Rad}^{-1})$		SCR, $\tau_0 K(\text{Rad}^{-1})$
	Const. V	Const. I	Const. I
1	$4.4 \cdot 10^{-8}$	$1.3 \cdot 10^{-9}$	*
2	$4.3 \cdot 10^{-8}$	$2.9 \cdot 10^{-9}$	*
66	$1.2 \cdot 10^{-7}$	$3.3 \cdot 10^{-8}$	$7.9 \cdot 10^{-9}$
68	$1.6 \cdot 10^{-7}$	$4.9 \cdot 10^{-8}$	$1.0 \cdot 10^{-8}$

\*At current considered, post-irradiation output exceeded pre-irradiation output.

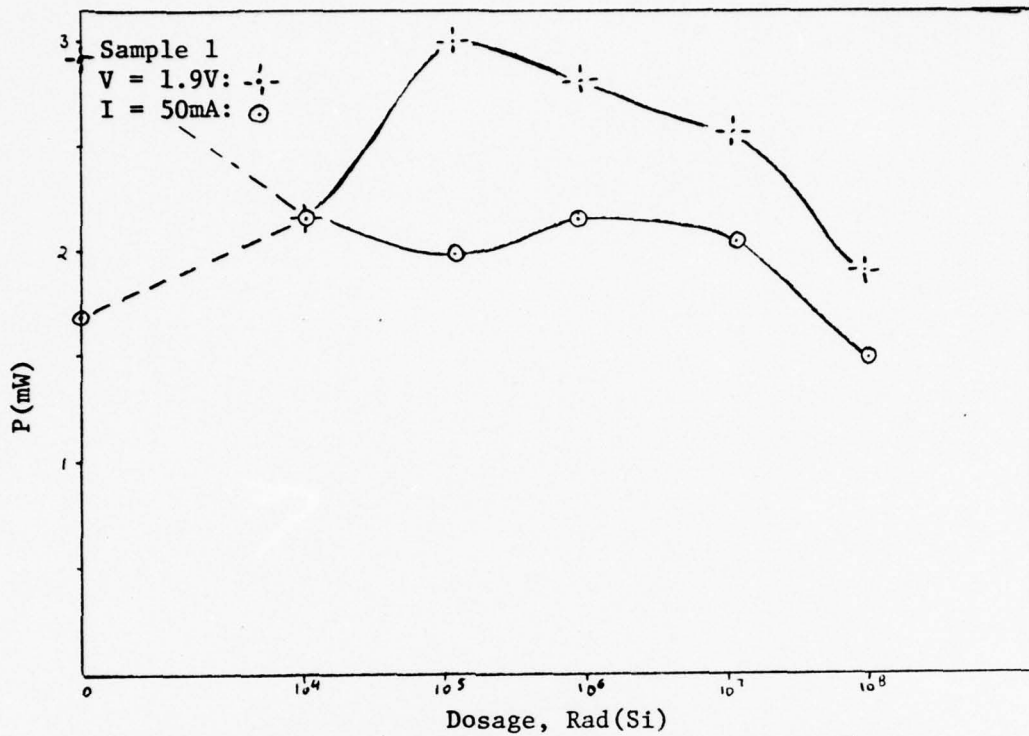


Fig. 15a. Constant Voltage and Constant Current Change in Power Output at 77°K

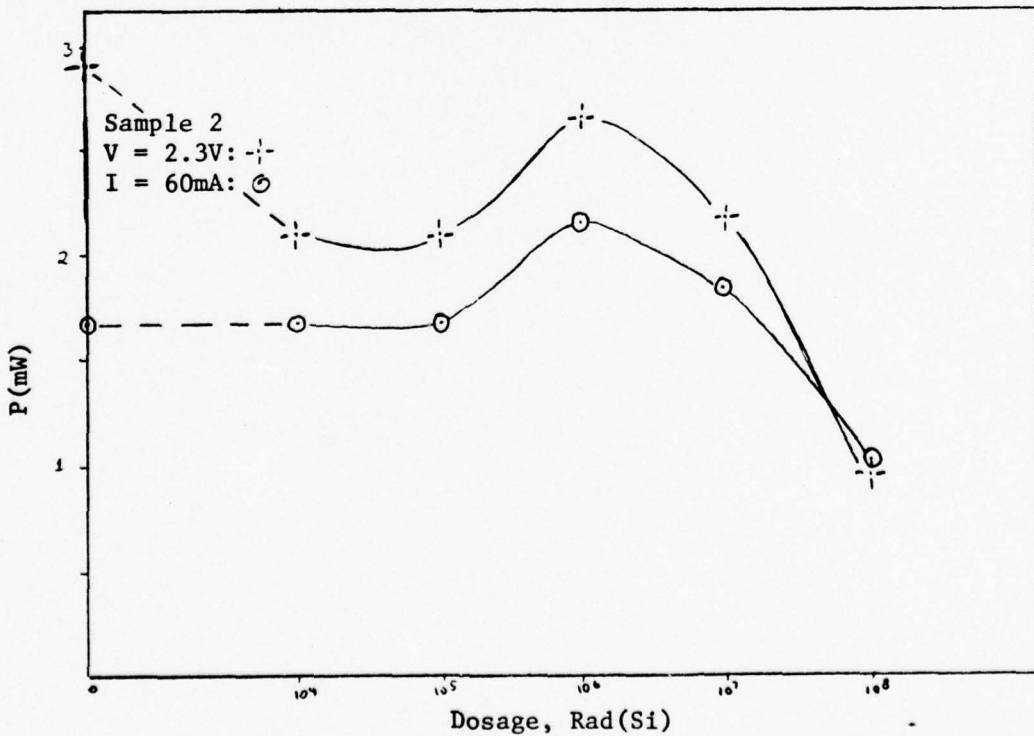


Fig. 15b. Constant Voltage and Constant Current Change in Power Output at 77°K

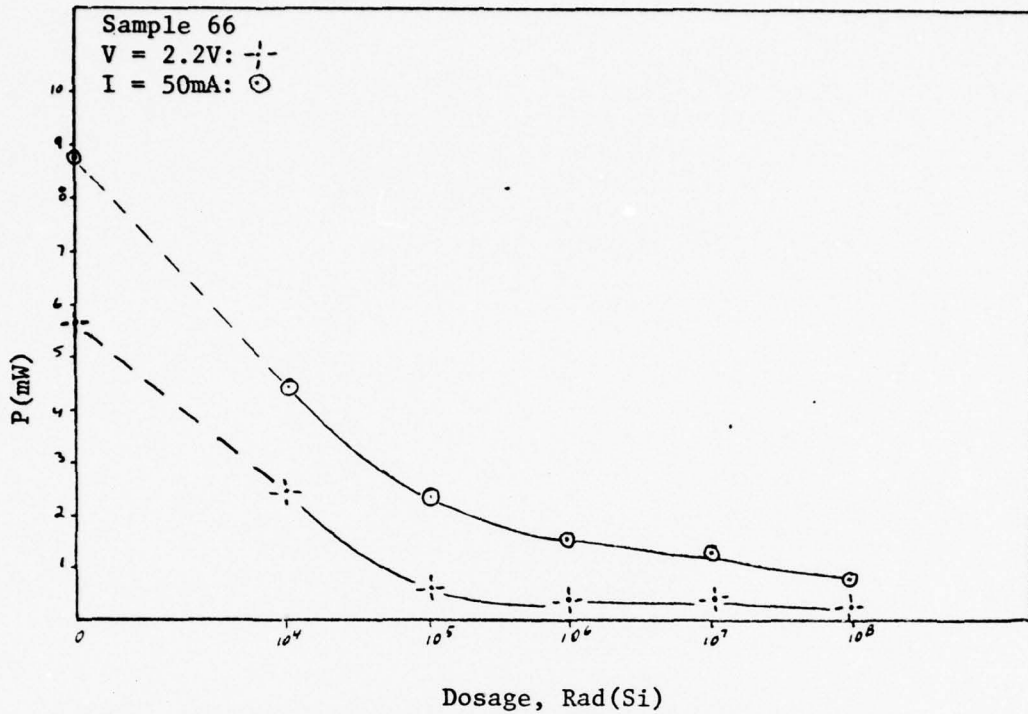


Fig. 15c. Constant Voltage and Constant Current Change in Power Output at 77°K

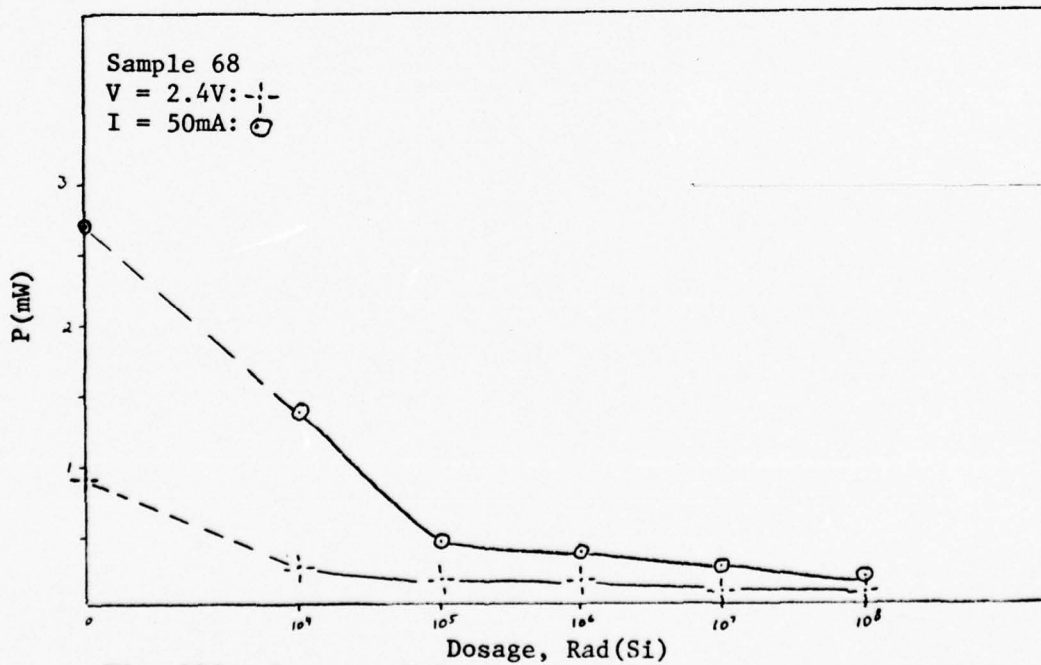


Fig. 15d. Constant Voltage and Constant Current Change in Power Output at 77°K

Since type LCW-10 diodes showed excellent radiation resistance, it was assumed for  $\tau_0K$  calculations that the radiative center profile was abrupt, or  $n = 0$ . For type C30127 the assumption was a linear profile, or  $n = 1$ . Based on the slopes of the output curves and the change in these curves with irradiation, a voltage value and a current value were selected where the radiative current appeared diffusion controlled in one case, and another set of values where the radiative current appeared to be due to SCR. Selection of these points was easily accomplished for type LCW-10 by examining Figs. 11 and 12. Including a  $\tau_0K$  value based on a radiative SCR mechanism for type C30127 was mainly for illustrative purposes, since Figs. 13 and 14 do not indicate, considering radiation effects, a region where the output is SCR controlled.

As expected, the damage factors for type LCW-10 were smaller by an order of magnitude than those obtained for type C30127. The difference in radiation sensitivity may be attributed to the factors discussed earlier.

### Efficiency

Radiation induced defects should have a direct effect on the efficiency of the device. Thus, if non-radiative recombination centers are introduced as a result of irradiation, the power efficiency, as well as the external differential quantum efficiency, is expected to decrease. Conversely, if the radiation induced defects act as radiative recombination centers, as proposed for type LCW-10, then an increase in efficiencies is expected. If, as has been suggested for type C30127, luminescent killer centers are introduced, then the decrease

in efficiency should be dramatic. Power efficiency at various dosages is presented in Figs. 16a - d.

Examination of Figs. 16a and b shows an increase in power efficiency to a dosage of  $10^6$ Rad(Si). This is in accordance with the proposed introduction of radiative recombination center defects. Figs. 16c and d show the rapid decline expected for a diffusion controlled output, light doping, and the possible introduction of luminescent killer centers.

#### Emission Peak Shift

The wavelength at the emission peak is presented in Table VIII as a function of dosage.

Determination of the emission peak was accomplished by examining spectral plots. The spectral plots were surrounded by an envelope and the highest point was chosen. This method is not considered to provide absolute information since it depends to a great extent on which particular mode was dominant at the time of the measurement. It does illustrate a general shift to higher energies, however. At higher dosages the spectra for Samples 66 and 68 were the result of spontaneous emission rather than stimulated emission, and consequently exhibited a rather broad, flat peak.

#### Intensity Distribution and Beam Divergence

The intensity distribution was measured for all samples prior to irradiation, and after  $10^6$ Rad(Si) for Samples 1 and 2 and  $5 \times 10^5$ Rad(Si) for Samples 66 and 68. In view of the radiation resistance exhibited by type LCW-10, no effect on the intensity distribution was expected for a dosage of  $10^6$ Rad(Si). The measurements verified this expectation

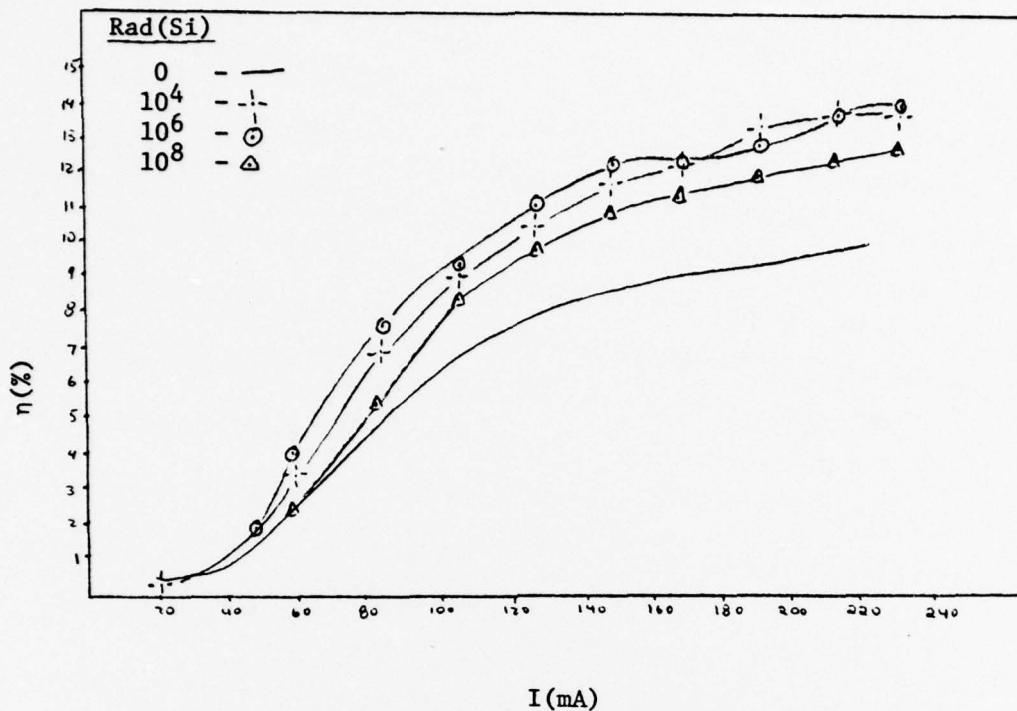


Fig. 16a. Power Efficiency at 77°K for Selected Dosages, Sample 1

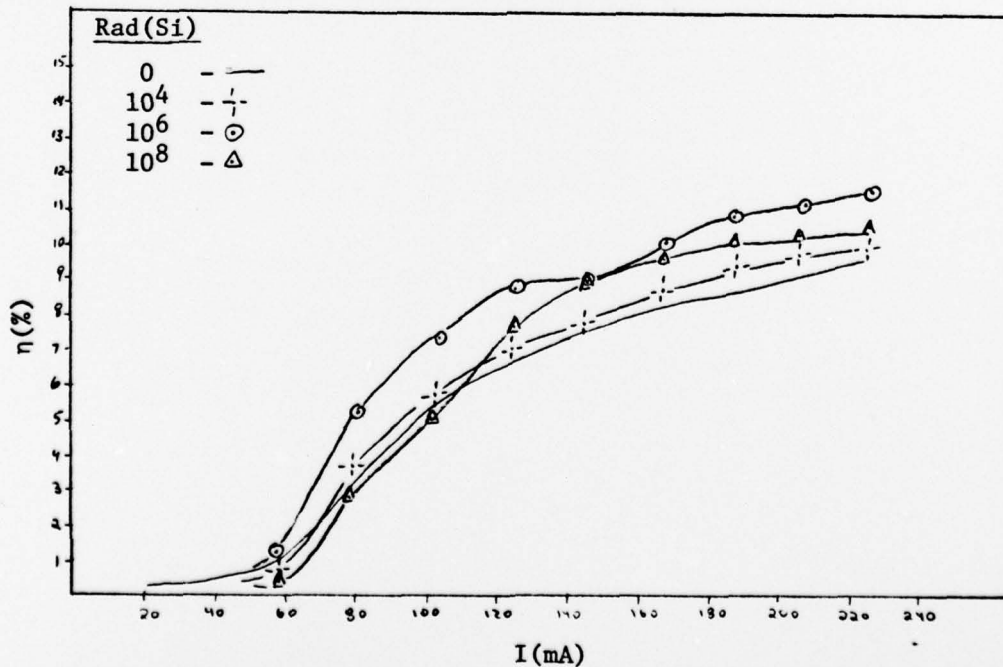


Fig. 16b. Power Efficiency at 77°K for Selected Dosages, Sample 2

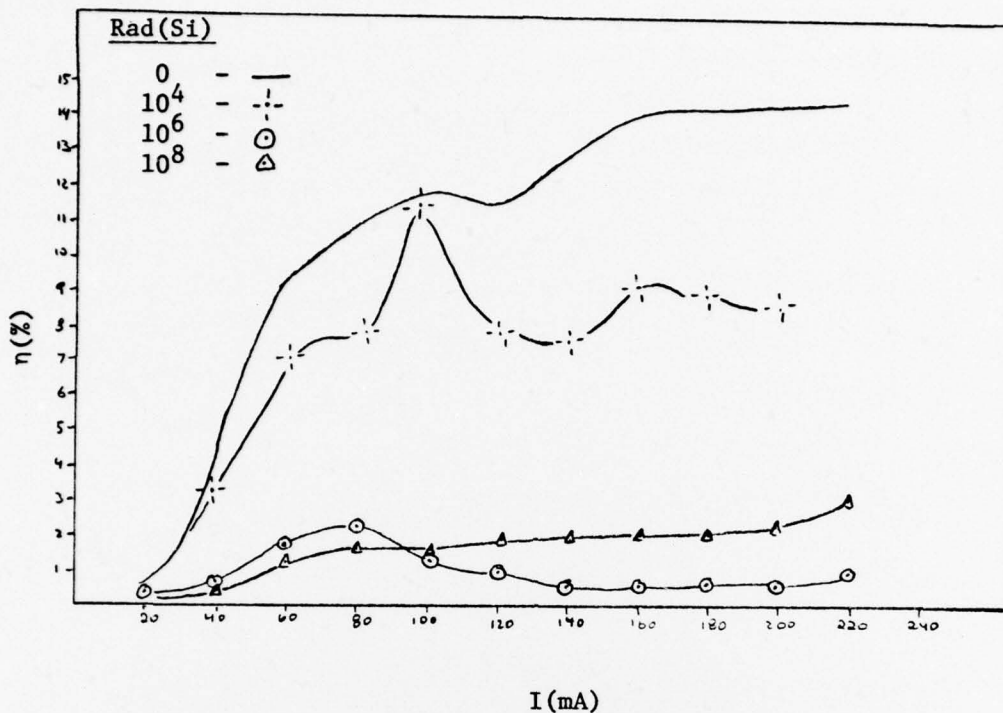


Fig. 16c. Power Efficiency at 77°K for Selected Dosages, Sample 66

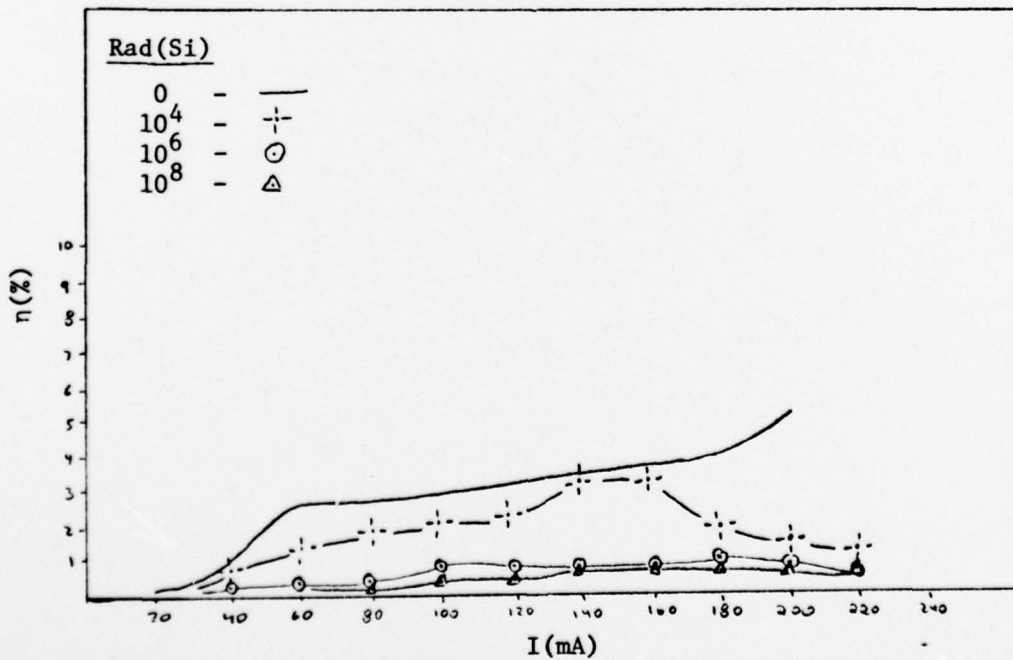


Fig. 16d. Power Efficiency at 77°K for Selected Dosages, Sample 68

Table VIII

Emission Peak Measured at Constant Current  
as a Function of Dosage

Sample Rad(Si)	Emission Peak (nm)			
	1	2	66	68
10	829.2	839.5	764.7	768.3
10 <sup>4</sup>	828.6	839.9	763.5	767.3
10 <sup>5</sup>	829.2	839.5	762.7	767.6
10 <sup>6</sup>	829.2	839.5	762.1	767.1
10 <sup>7</sup>	829.5	839.5	762.3	767.1
10 <sup>8</sup>	828.1	839.0	762.3	767.6

as illustrated in Figs. 17 and 18. The effect of radiation on type C30127 was so pronounced in all respects, that the drastic change in intensity distribution, as illustrated in Figs. 19 and 20, was not entirely surprising. A possible explanation may be that the radiation changed the configuration of the active region by the introduction of a large number of non-radiative centers, which in turn decreased the region where gain was high enough for lasing to occur. The beam divergence is presented in Table IX, and supports the idea of a changed active region for type C30127.

Table IX

Beam Divergence Before and After Irradiation

Sample*	Beam Divergence (degrees, HWHM)		
	Calculated	Pre-Irrad	Post-Irrad**
1	4	3	3
⊥	-	22	19
2	4	12	11
⊥	-	19	16
66	4	4	19
⊥	23	17	19
68	4	10	23
⊥	23	26	18

\* || and ⊥ indicate parallel and perpendicular to the junction plane respectively.

\*\*10<sup>6</sup>Rad(Si) for Samples 1 and 2; 5x10<sup>5</sup>Rad(Si) for Samples 66 and 68.

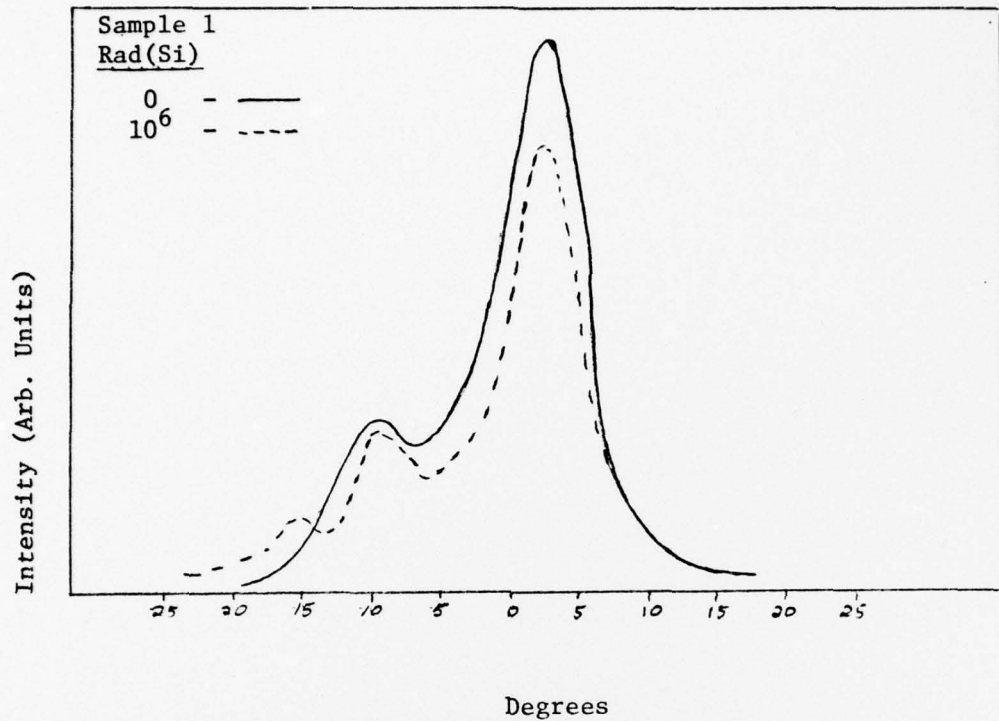


Fig. 17a. Intensity Distribution in Far Field, Pre- and Post-Irradiation, Parallel to Junction

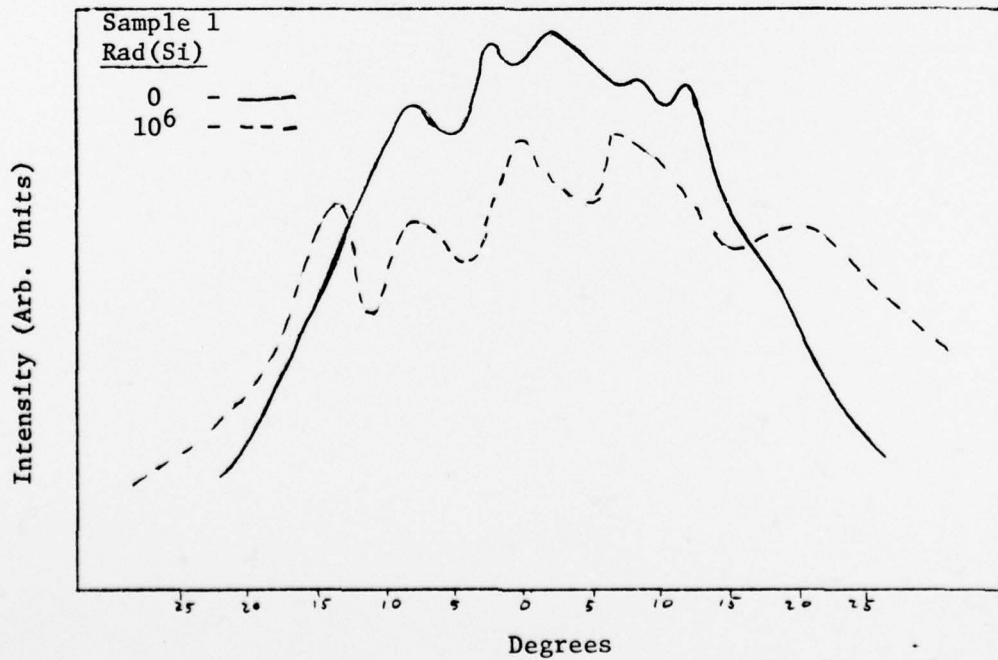


Fig. 17b. Intensity Distribution in Far Field, Pre- and Post-Irradiation, Perpendicular to Junction

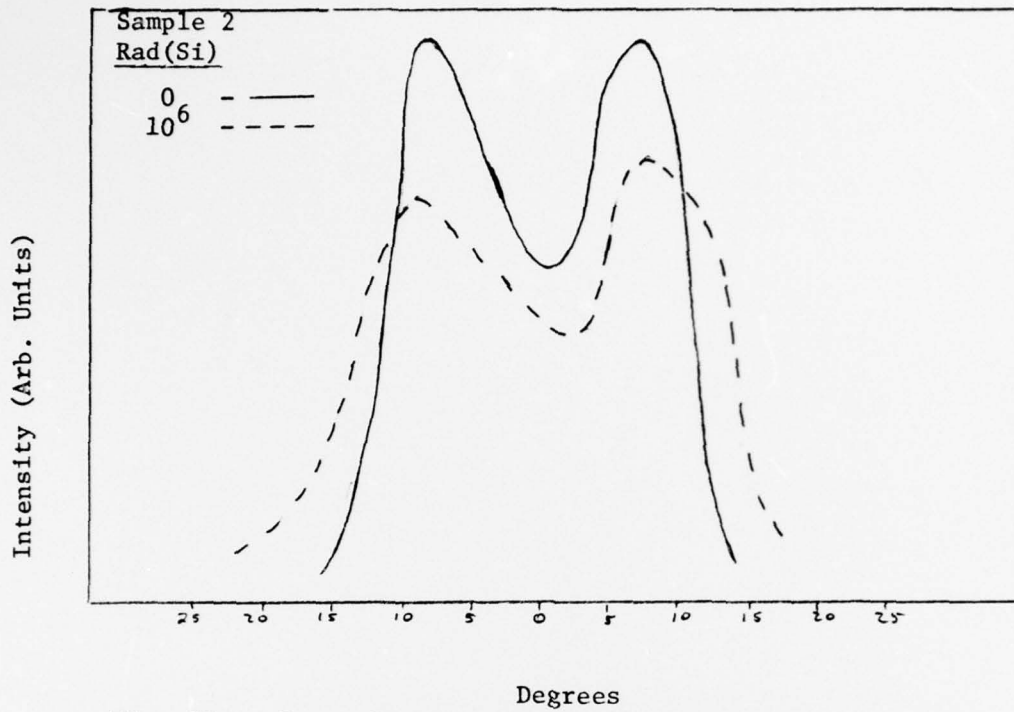


Fig. 18a. Intensity Distribution in Far Field, Pre- and Post-Irradiation, Parallel to Junction

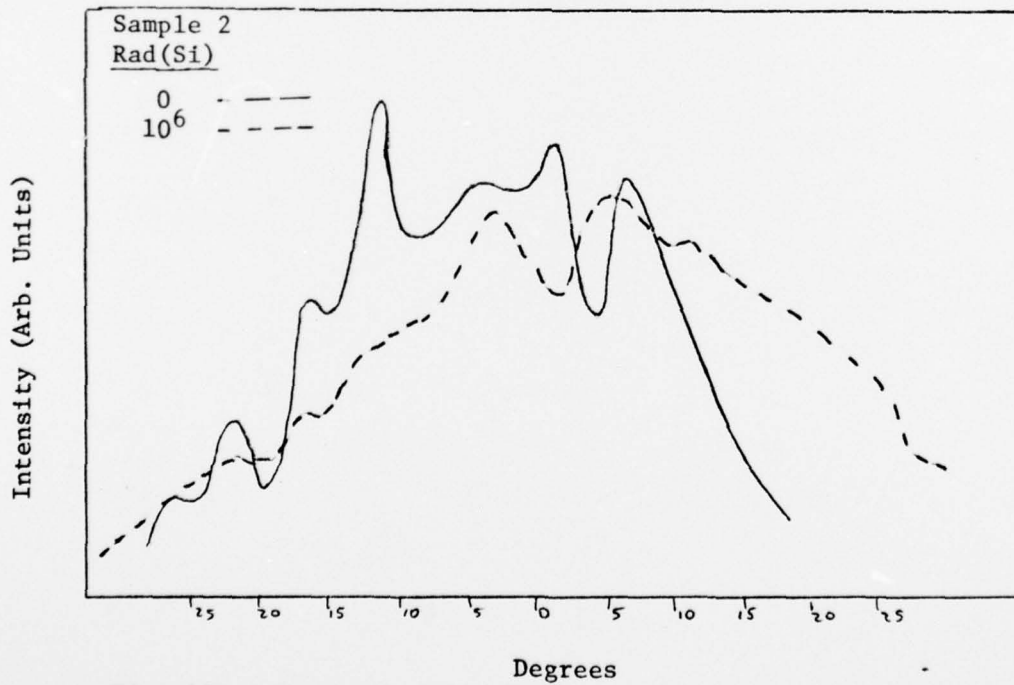


Fig. 18b. Intensity Distribution in Far Field, Pre- and Post-Irradiation, Perpendicular to Junction

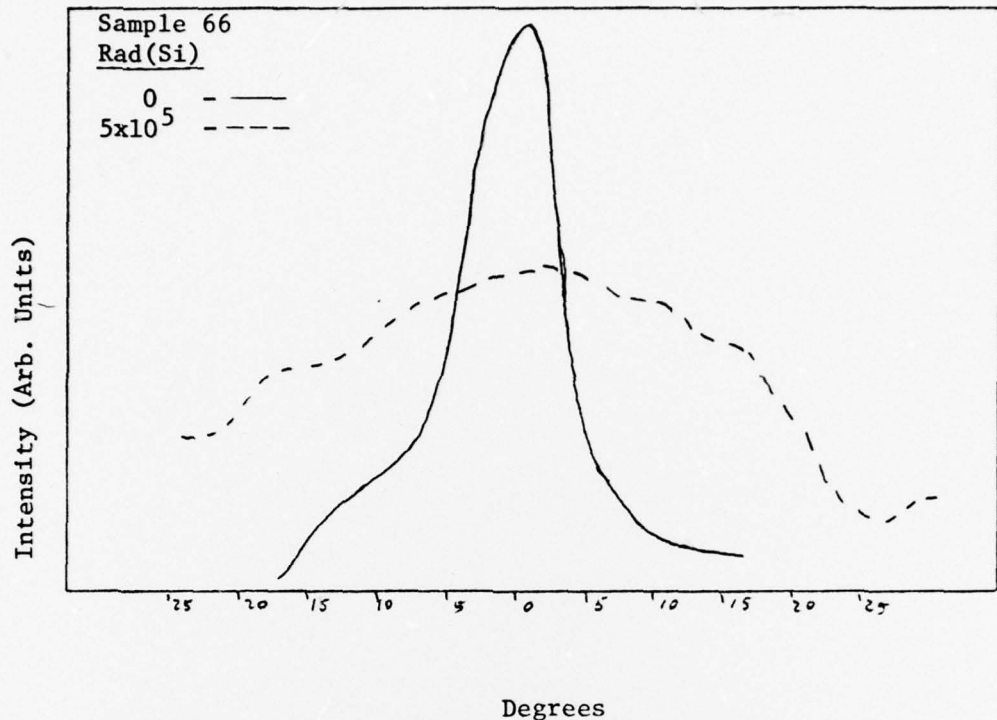


Fig. 19a. Intensity Distribution in Far Field, Pre- and Post-Irradiation, Parallel to Junction

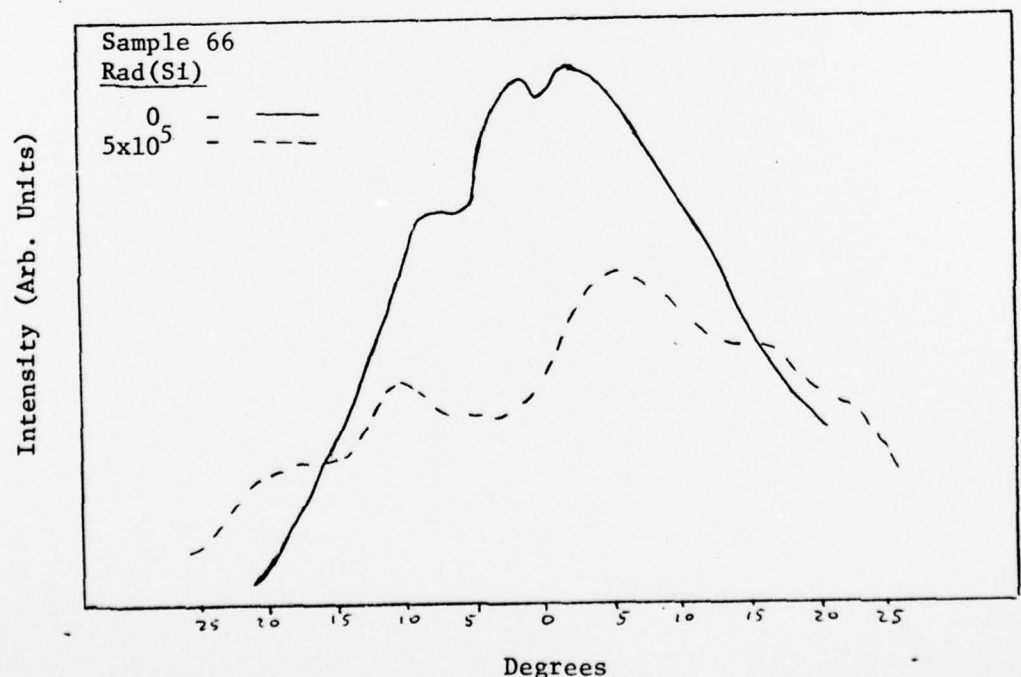


Fig. 19b. Intensity Distribution in Far Field, Pre- and Post-Irradiation, Perpendicular to Junction

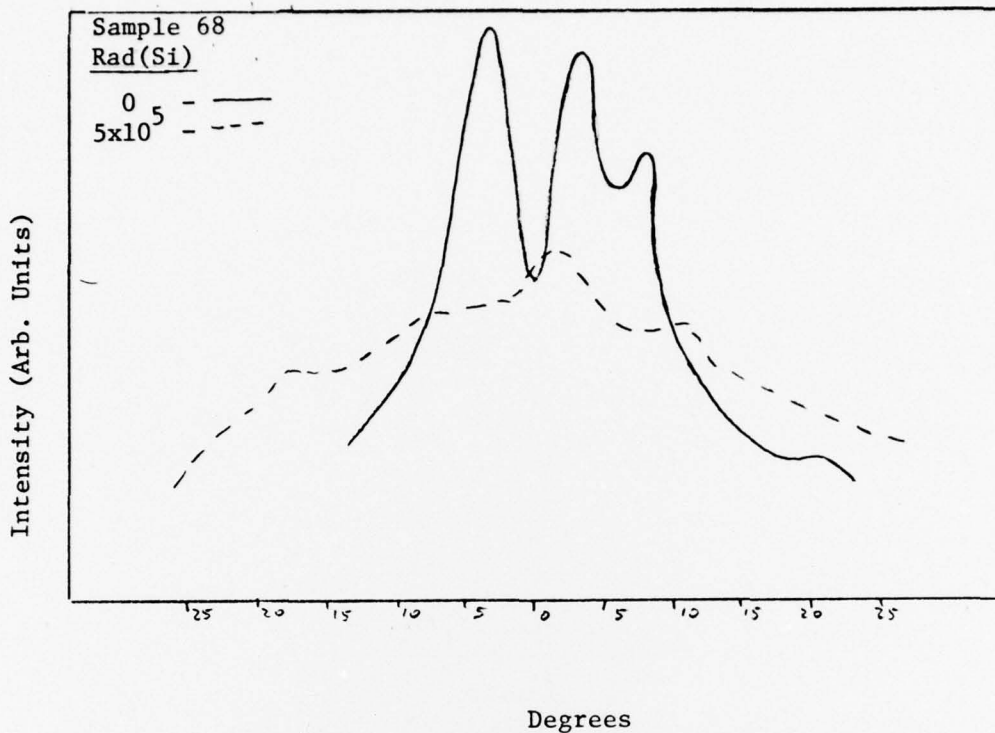


Fig. 20a. Intensity Distribution in Far Field, Pre- and Post-Irradiation, Parallel to Junction

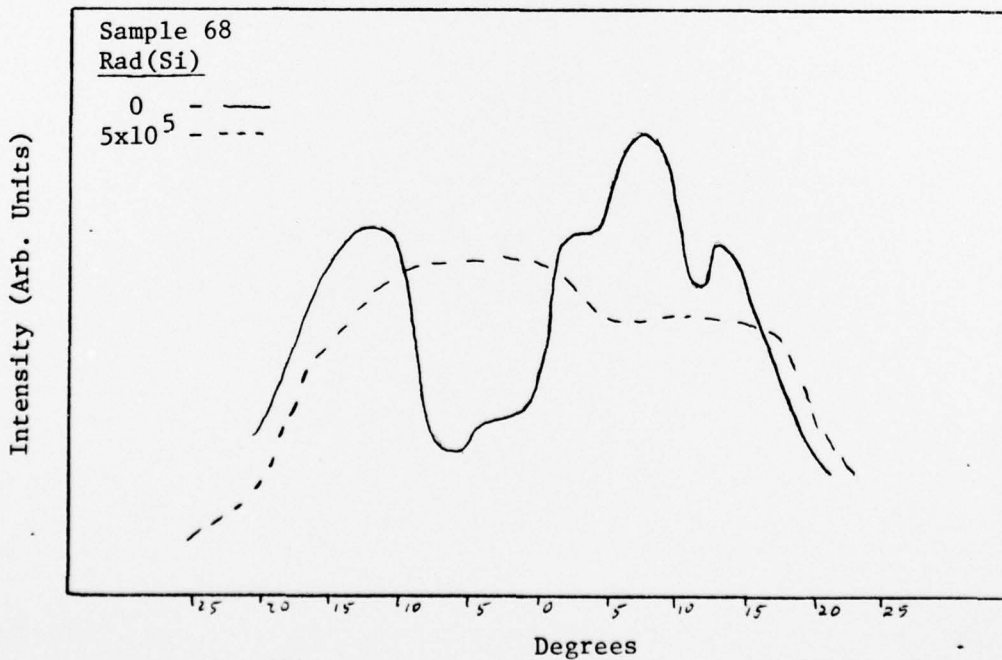


Fig. 20b. Intensity Distribution in Far Field, Pre- and Post-Irradiation, Perpendicular to Junction

For the perpendicular spread in the case of Samples 1 and 2 the single slit diffraction approximation breaks down. With that exception, good agreement exists between calculated and measured pre-irradiation values. The proposed change in the extent of the active region falls in line with the measured post-irradiation values. The introduction of additional radiative centers could serve to widen the region and thus result in less beam divergence as appears to have happened for the spread in Samples 1 and 2. Conversely, the severe reduction of radiative centers in the case of Samples 66 and 68, could reduce the extent of the active region and result in large values of divergence. According to the measured values, using the narrow slit approximation, the width of the active region in Samples 66 and 68 was reduced to a value near the thickness, so that the light, instead of being emitted by a narrow slit, is actually being emitted by a small rectangular aperture.

## V. Conclusions

The primary conclusion is that the injection lasers of type LCW-10 are much more resistant to irradiation by a gamma source than type C30127.

Type LCW-10 exhibited increased light output to  $10^6$ Rad(Si), and at  $10^8$ Rad(Si) still performed at levels comparable to pre-irradiation values. The value of the threshold current did not noticeably change as a result of irradiation, nor were the intensity distribution and beam divergence significantly affected. Along with the increase in output, power and external differential quantum efficiency increased initially.

The performance degradation of type C30127 proceeded rapidly in all respects. Output decreased by a factor of two after only  $10^4$ Rad(Si), threshold current increased, efficiencies decreased, and beam characteristics changed drastically.

Without knowledge of device composition and structure, some assumptions were made. The calculated damage factors show these assumptions to be reasonably valid. It is believed that the output of type LCW-10 is due to SCR while type C30127 is diffusion controlled. Additionally, it is thought that the former is heavily doped while the latter is only lightly doped.

The quantitative results given throughout this study are believed to accurately represent radiation induced performance changes in the two types of injection lasers. Since the investigation was concerned only with two specific types, the results apply only to them, and even then should be used with care since only two samples of each type were tested.

## VI. Recommendations

The data obtained in this study are of necessity quantitative only. Interpretation of experimental results had to be largely based on assumptions about device composition. In view of this, it was not possible to assign a specific result to a definite physical process or mechanism.

If detailed information could be obtained from the respective manufacturers, a physical interpretation of the results may be possible. This information, in turn, could serve to possibly create devices of even greater radiation hardness than the present type LCW-10. Additionally, the effects of radiation other than gamma should be investigated, since results could differ considerably.

Another area to be investigated concerns the annealing behavior, either due to forward bias or elevated temperatures. This could provide further insight into the physical processes occurring within each device.

### Bibliography

1. Aukerman, L. W., et al. "Radiation Effects in GaAs." Journal of Applied Physics, 34-12:3590-3599 (December 1963).
2. Aukerman, L. W., et al. "Effects of Radiation Damage on the Behavior of GaAs p-n Junctions." IEEE Transactions on Nuclear Science, NS13-6:174-180 (December 1966).
3. Barnes, C. E. "Effects of Co<sup>60</sup> Gamma Irradiation in Epitaxial GaAs Laser Diodes." Physical Review, 1-12:4735-4747 (June 1970).
4. Campos, M. D., et al. "Cavity Competition in Anomalous Emission Intensity in Double-Heterostructure (DH) Lasers." IEEE Journal of Quantum Electronics, QE13-8:687-691 (August 1977).
5. Compton, D. M. J. and R. A. Cesena. "Mechanisms of Radiation Effects on Lasers." IEEE Transactions on Nuclear Science, NS14-6:55-61 (December 1967).
6. Kabayashi, K., et al. "Unstable Horizontal Transverse Modes and Their Stabilization with a New Stripe Structure." IEEE Journal of Quantum Electronics, QE13-8:659-661 (August 1977).
7. Pankove, J. I. Optical Processes in Semiconductors. New York: Dover Publications, Inc., 1975.
8. Saji, M. and Y. Inuishi. "Radiation Damage and Annealing of GaAs Laser Diode." Japanese Journal of Applied Physics, 4:830-831 (1965).
9. Share, S. et al. "Properties of Compensated GaAs Light-Emitting Diodes Following <sup>60</sup>Co Irradiation." Solid State Electronics, 18:471-480 (1975).
10. Stanley, A. G. "Comparison of Light-Emitting Diodes in a Space Radiation Environment." IEEE Transactions on Nuclear Science, NS17-6:239 (1970).
11. Sze, S. M. Physics of Semiconductors. New York: Wiley Interscience, 1969.

### Vita

Harro Ackermann was born on 4 March 1942 in Magdeburg, Germany. He attended schools in Germany until coming to the United States in 1956. In 1960 he graduated from Richland High School, Richland, Missouri. He entered the University of Maryland/Munich in 1962, transferred to the Missouri School of Mines and Metallurgy in 1964, and was awarded a Bachelor of Science Degree from that institution in May 1966. Following graduation he was employed as an Associate Engineer at McDonnell-Douglas Company, St. Louis, Missouri until entering Officer Training School, Lackland Air Force Base, Texas, in 1967. His Air Force assignments in the United States, Germany, and Turkey were all in the space defense field. He was assigned to the Air Force Institute of Technology in June 1976.

This thesis was typed by Mrs. Anna L. Lloyd.

Unclassified

SECURITY CLASSIFICATION OF THIS PAGE (When Data Entered)

REPORT DOCUMENTATION PAGE		READ INSTRUCTIONS BEFORE COMPLETING FORM
1. REPORT NUMBER AFIT GEP/PH/77-1	2. GOVT ACCESSION NO.	3. RECIPIENT'S CATALOG NUMBER
4. TITLE (and Subtitle) EFFECTS OF GAMMA RADIATION ON GALLIUM-ARSENIDE LASERS.	5. TYPE OF REPORT & PERIOD COVERED MS Thesis Master's thesis	6. PERFORMING ORG. REPORT NUMBER
7. AUTHOR(s) Harro Ackermann Captain, USAF	8. CONTRACT OR GRANT NUMBER(s)	
9. PERFORMING ORGANIZATION NAME AND ADDRESS Air Force Institute of Technology (AFIT-EN) Wright-Patterson AFB, OH 45433	10. PROGRAM ELEMENT, PROJECT, TASK AREA & WORK UNIT NUMBERS	
11. CONTROLLING OFFICE NAME AND ADDRESS	12. REPORT DATE Dec 1977	13. NUMBER OF PAGES 62
14. MONITORING AGENCY NAME & ADDRESS (if different from Controlling Office)	15. SECURITY CLASS. (of this report) Unclassified	15a. DECLASSIFICATION/DOWNGRADING SCHEDULE
16. DISTRIBUTION STATEMENT (of this Report) Approved for public release; distribution unlimited		
17. DISTRIBUTION STATEMENT (of the abstract entered in Block 20, if different from Report)		
18. SUPPLEMENTARY NOTES Approved for public release; IAW AFR 190-17 JERRAL F. GUESS, Captain, USAF Director of Information		
19. KEY WORDS (Continue on reverse side if necessary and identify by block number) Radiation Damage Radiation Effects Injection Lasers D12 225		
20. ABSTRACT (Continue on reverse side if necessary and identify by block number) The effect of gamma radiation from a Co <sup>60</sup> source on the performance of two types of aluminum gallium arsenide injection lasers was investigated. Both types of lasers were designed to operate in the continuous wave mode at room temperature. Measurements were conducted to determine radiation induced changes in the threshold current, power output, efficiency, and spectral and intensity distributions. Damage factors were calculated by the constant voltage and constant		

DD FORM 1 JAN 73 1473

EDITION OF 1 NOV 65 IS OBSOLETE

Unclassified

SECURITY CLASSIFICATION OF THIS PAGE (When Data Entered)

current methods.

Type C30127 (RCA) exhibited rapid degradation. A dosage of  $10^4$  Rad(Si) reduced the output power by a factor of two. Threshold current increased, efficiency decreased, and the intensity distribution changed drastically. The damage factor at constant voltage was calculated to be  $1.5 \times 10^{-7}$  Rad<sup>-1</sup>.

The performance of LCW-10 (Laser Diode Laboratories, Inc.) improved to a dosage of  $10^6$  Rad(Si) before the onset of degradation. After  $10^8$  Rad(Si) power output was still comparable to pre-irradiation values. No significant changes in beam characteristics were noted. The damage factor at constant voltage was  $4 \times 10^{-8}$  Rad<sup>-1</sup>.

MEGA RAD